Title
Layer 4 Gates Plasticity in Visual Cortex Independent of a Canonical Microcircuit

Journal
Current Biology, 30(15)

ISSN
0960-9822

Authors
Frantz, Michael G
Crouse, Emily C
Sokhadze, Guela
et al.

Publication Date
2020-08-01

DOI
10.1016/j.cub.2020.05.067

HHS Public Access

Author manuscript

Curr Biol. Author manuscript; available in PMC 2021 August 03.

Published in final edited form as:

Curr Biol. 2020 August 03; 30(15): 2962–2973.e5. doi:10.1016/j.cub.2020.05.067.

Layer 4 gates plasticity in visual cortex independent of a canonical microcircuit

Michael G. Frantz[2,†], **Emily C. Crouse**[1,†], **Guela Sokhadze**[1,†], **Taruna Ikrar**[3], **Céleste-Élise Stephany**[2], **Collins Nguyen**[3], **Xiangmin Xu**[3,*], **Aaron W. McGee**[1,2,4,*]

[1]Department of Anatomical Sciences and Neurobiology, School of Medicine, University of Louisville, Louisville, Kentucky, 40202

[2]Developmental Neuroscience Program, Saban Research Institute, Children's Hospital Los Angeles, Department of Pediatrics, Keck School of Medicine, University of Southern California, Los Angeles, California 90027, USA.

[3]Department of Anatomy and Neurobiology, School of Medicine, University of California, Irvine, CA 92697, USA

[4]Lead contact

Summary

Disrupting binocular vision during a developmental critical period can yield enduring changes to ocular dominance (OD) in primary visual cortex (V1). Here we investigated how this experience-dependent plasticity is coordinated within the laminar circuitry of V1 by deleting separately in each cortical layer (L) a gene required to close the critical period, *nogo-66 receptor* (*ngr1)*. Deleting *ngr1* in excitatory neurons in L4, but not in L2/3, L5, or L6, prevented closure of the critical period and adult mice remained sensitive to brief monocular deprivation. Intracortical disinhibition but not thalamocortical disinhibition accompanied this OD plasticity. Both juvenile wild-type mice and adult mice lacking *ngr1* in L4 displayed OD plasticity that advanced more rapidly L4 than L2/3 or L5. Interestingly, blocking OD plasticity in L2/3 with the drug AM-251 did not impair OD plasticity in L5. We propose that L4 restricts disinhibition and gates OD plasticity independent of a canonical cortical microcircuit.

eTOC Blurb

Frantz *et al*. explore the regulation and propagation of experience-dependent plasticity within the laminar circuitry of visual cortex. Layer 4 limits intracortical disinhibition to close the critical

*Correspondence to: xiangmix@uci.edu and aaron.mcgee@louisville.edu.
†These authors contributed equally to this work

Author Contributions

The contributions are as follows: MGF, ECC, GS, XX, and AWM designed the study. MGF, ECC, GS, CES, and TI performed the experiments. CN assisted with data analysis. XX and AWM wrote the manuscript.

Declaration of Interests

The authors declare no competing interests

period for OD plasticity throughout visual cortex. OD plasticity does not follow a canonical cortical microcircuit.

Introduction

Ocular dominance (OD) in primary visual cortex (V1) is a premier model for studying experience-dependent plasticity in cortical circuitry. Brief durations of monocular deprivation (MD) during development shift neuronal responses to favor the non-deprived eye in numerous species including cat, primate, and rodent [1–4]. This plasticity is confined to a developmental critical period extending from approximately postnatal (P) day 19 to 32 in the mouse [5]. MD spanning this critical period results in permanent impairments in eye dominance [6]. Both synaptic and structural plasticity are proposed to contribute to OD plasticity [6–9], but how visual experience drives long-lasting changes in cortical circuits remains only partially understood.

Several studies have demonstrated that visual plasticity during the critical period results from a decrease in cortical responses to visual stimuli presented to the deprived eye. By comparison, a weaker form of OD plasticity in adult mice requires longer durations of MD and predominantly relies on potentiation of responses to the non-deprived eye [10–12]. Interestingly, a diversity of environmental, pharmacologic, and genetic manipulations all enhance OD plasticity in adult mice [13]. Many of these approaches for ‘reactivating’ OD plasticity appear to converge on increasing the relative strength of excitatory to inhibitory neurotransmission (E/I ratio) [14]. However, where within the circuitry of V1 these manipulations operate to re-open the critical period has not been determined.

How OD plasticity emerges and propagates within the laminar circuitry of V1 remains controversial. In kittens, one day of MD yields substantial shifts in L2/3 and L5/6 towards the non-deprived eye while the binocularity of L4 is preserved [15]. In mice, one study has reported that L2/3 and L4 exhibit OD plasticity simultaneously, but did not measure plasticity in L5 [16]. Understanding how OD plasticity is coordinated across cortical layers may provide insight into the cellular and signaling mechanisms that limit cortical plasticity and lead to strategies that promote experience-dependent plasticity for therapeutic gain.

To explore the rules governing OD plasticity, here we exploited the requirement for the *ngr1* gene to close the critical period. NgR1 is enriched at excitatory synapses but localizes to both axons and dendrites [17]. It is a receptor for several inhibitors of axon outgrowth associated with central nervous system myelin [18]. OD plasticity observed in adult *ngr1* −/− mice (P60–90) is as yet indistinguishable from juvenile WT mice (P19–32) [19]. During the critical period, 4 days of MD yields a maximal shift in eye dominance towards the non-deprived eye [5]. Adult *ngr1* −/− mice exhibit similar OD shifts with 4 days of MD (P60–90) [20,21]. OD plasticity for both juvenile WT mice and adult *ngr1* −/− mice is resistant to benzodiazepines and barbiturates [12,19,20,22]. Moreover, MD promotes disinhibition within cortical circuitry in both juvenile WT mice and adult *ngr1* −/− mice. This disinhibition is mediated by a reduction of excitatory drive onto interneurons expressing parvalbumin (PV) [19,23,24]. Here we probed the characteristics of OD plasticity by deleting *ngr1* selectively within different cortical layers.

Results

Restricting deletion of *ngr1* to neocortex permits OD plasticity in adult mice

We dissected the expression requirement for *ngr1* to close the critical period by deleting the gene within different populations of excitatory neurons through a conditional allele (*ngr1 flx*). In this allele, *loxP* sites flank the second exon that contains the entire protein coding sequence of the mature receptor. Cre recombinase deletes this region to abolish the expression of NgR1 protein and to initiate the expression of enhanced green fluorescent protein (GFP) from a reporter cassette containing the splice acceptor sequence of *ngr1* exon 2 (Figure S1; related to Figure 1) [25]. In the absence of Cre recombinase, GFP expression is not detectable by immunofluorescence staining of coronal brain sections or by immunoblot [26].

OD plasticity is expressed in V1 where inputs from monocular neurons residing in different laminae of the lateral geniculate nucleus (LGN) of the thalamus are combined. In the mouse, the separation of thalamic inputs is less distinct than in cats or primates, but relay neurons in LGN conveying information from each eye similarly converge in the binocular zone of V1. A characteristic of mice is overall greater responses to visual input from the contralateral eye [5,27]. WT mice possess contralateral bias index (CBI) values that typically range from 0.65 to 0.75 as calculated from multi-unit electrophysiologic recordings with high impedance electrodes (10 mega-ohm or greater) across the depth of V1 (CBI = 0.68 ± .05, n = 5) (Figure 1A) [21]. Following 4–5 days of MD during the critical period (P27–32), WT mice display OD plasticity that shifts eye dominance towards the non-deprived eye (4-day MD juvenile WT, CBI = 0.52 ± .05, n = 8) (P=.034, Kruskal-Wallis test with Dunn's correction (KW test) for each of 3 genotypes comparing non-deprived vs. 4-day MD) (Figure 1A, Figure S1).

We deleted *ngr1* throughout neocortex with *CamK2a-Cre* (*L2–6-Cre*) to determine if restricting the deletion of *ngr1* to excitatory cortical neurons would permit OD plasticity in adult mice after the close of the critical period. This transgene expresses Cre recombinase in excitatory neurons in layers (L) L2 through L6 of cerebral cortex but not in thalamic nuclei [28]. Adult *ngr1 flx/flx; L2–6-Cre* mice exhibited OD plasticity with MD (CBI = 0.41 ± .05; n = 5), and their CBI values were significantly lower than those of non-deprived *ngr1 flx/flx; L2–6-Cre* control mice (CBI = .73 ± .04; n = 4, P=.004, KW test) (Figure 1A). This OD plasticity is comparable to that observed in both juvenile WT mice and adult *ngr1 −/−* mice (non-deprived KO CBI = .65 ± .04 vs. 4-day MD KO CBI = .42 ± .11, P = .024, KW test) (Figure 1A) [5,20].

Juvenile WT mice display OD plasticity in every cortical layer [5]. To measure OD plasticity in different cortical layers, we examined Ocular Dominance Index (ODI) scores at recording depths from the pial surface corresponding to L2/3 (150–300 microns), L4 (350–450 microns), and L5 (550–750 microns) (Figure 1B) [29]. Comparing the cumulative distributions of ODI scores for non-deprived *ngr1 flx/flx; L2–6 Cre* mice and *ngr1 flx/flx; L2–6 Cre* mice receiving 4 days of MD revealed significant OD plasticity in each cortical layer (P < .0001, KW test for each layer between non-deprived and 4-day MD groups) (Figure 1B). Thus, selective deletion of *ngr1* in excitatory cortical neurons is sufficient to

permit OD plasticity throughout V1 that is otherwise confined to a developmental critical period.

L4 gates the critical period for OD plasticity

We considered three possible outcomes for deleting *ngr1* from excitatory neurons separately in each cortical layer. First, if deleting *ngr1* from most cortical excitatory neurons is required to prevent the critical period from closing, as we observe in *ngr1 flx/flx; L2–6 Cre* mice, then restricting deletion of *ngr1* to any cortical layer would not be sufficient to permit OD plasticity in adult mice. The distribution of ODI scores following 4–5 days of MD in mice lacking *ngr1* in any single layer would be indistinguishable from *ngr1 flx/flx* mice not expressing Cre. This would also be the expected outcome if expression of *ngr1* in any layer is sufficient to close the critical period. Second, if the *ngr1* gene limits OD plasticity in a cell-autonomous manner, then only excitatory neurons expressing Cre and lacking *ngr1* would exhibit shifts in eye dominance with brief MD. The layer expressing Cre would display OD plasticity. This observation would also reveal that each layer responds to MD independent from the surrounding layers. Third, if one or more layers gates the critical period, then deleting *ngr1* in that layer would yield OD plasticity throughout V1 similar to adult *ngr1 −/−* and *ngr1 flx/flx; L2–6-Cre* mice.

To delete *ngr1* from excitatory neurons in different cortical layers we employed *in utero* electroporation and several characterized Cre ‘driver’ lines (Figure 2A and S2). As neurons residing in L2/3 are the last population to be born and migrate from the subventricular zone during early development [30], we performed *in utero* electroporation (IUEP) on embryonic day (E) 15.5 *ngr1 flx/flx* pups to transfect nascent L2/3 neurons with a plasmid containing Cre-GFP under a beta-actin promoter (*L2/3-Cre*) [31,32]. Consistent with published findings [33], we observed extensive labeling of neurons in L2/3 of V1 with antibodies directed against GFP in coronal sections from these mice receiving IUEP (Figure 2A). We estimate that at least 30% of excitatory neurons in L2/3 expressed Cre-GFP. To delete *ngr1* selectively in either L4, L5, or L6, we employed characterized transgenic Cre drivers selective for each layer: *Scnn1a-Tg3-Cre* for L4 (*L4-Cre*), *Rpb4a-Cre* for L5 (*L5-Cre*), and *Ntsr1-Cre* for L6 (*L6-Cre*) [34–36]. *Scnn1a-Tg3-Cre* is expressed by approximately 60% of excitatory neurons in L4 and *Rbp4a-Cre* is expressed by an estimated 40% of excitatory neurons in L5 [37]. *Ntsr1-Cre* confines expression to corticothalamic projection neurons that represent approximately 65% of excitatory neurons in L6 [38]. These Cre drivers induced the expression of GFP from the recombined *ngr1 flx* gene locus in a layer-restricted manner that mirrors the expression patterns of Cre recombinase established with the Cre reporter line *Ai14 (Tdtomato)* (Figure 2A) [34,39].

Comparing the effects of MD on adult mice lacking *ngr1* in L2/3, L4, L5, or L6, revealed that L4 gates OD plasticity (Figure 2B). We measured eye dominance in adult mice following 4 days of MD (P60–90) with multi-unit electrophysiologic recordings and high impedance electrodes. Deleting *ngr1* in L2/3 did not yield detectable OD plasticity. CBI values for these mice were comparable to *ngr1 flx/flx* mice that did not express Cre (*ngr1 flx/flx, L2/3-Cre* CBI = 0.67 ± .06, n = 7, vs. *ngr1 flx/flx*; CBI = 0.71 ± .07, n = 8, P > .99; KW test comparing *ngr1 flx/flx* vs. *L/23-Cre*, *L4-Cre*, *L5-Cre*, and *L6-Cre,* and *L4-Cre* non-

deprived vs. 4-day MD *L4-Cre* and *ngr1 flx/flx*) (Figure 2A and S2). In contrast, deleting *ngr1* in L4 permitted in OD plasticity. CBI scores for *ngr1 flx/flx; L4-Cre* adult mice following 4 days of MD were significantly lower than *ngr1 flx/flx* mice (*ngr1 flx/flx, L4-Cre* CBI = 0.45 ± .09, n = 8; P = .005, KW test) and non-deprived *ngr1 flx/flx; L4-Cre* adult mice (non-deprived *ngr1 flx/flx, L4-Cre* CBI = 0.71 ± .07, n = 5; P = .006, KW test). Non-deprived control *ngr1 flx/flx; L4-Cre* adult mice displayed normal eye dominance (P > .99, KW test). Deleting *ngr1* in L5 or L6 did not permit OD plasticity in adult mice following MD (*ngr1 flx/flx, L5-Cre* CBI = 0.70 ± .08, n = 8; *ngr1 flx/flx, L6-Cre* CBI = 0.71 ± .03, n = 8, P > .99; KW test).

To determine whether the CBI scores for individual mice did not reflect OD plasticity from neurons in the layer expressing Cre, we examined the cumulative distribution of ODI scores for each cortical layer (KW test for each layer comparing *ngr1 flx/flx* vs. *L/23-Cre*, *L4-Cre*, *L5-Cre*, and *L6-Cre*) (Figure 2C–E). Neurons in the layer expressing Cre did not display OD plasticity for *L/23-Cre*, *L5-Cre*, or *L6-Cre* mice. The distribution of ODI scores following 4 days of MD for *ngr1 flx/flx* mice, and *ngr1 flx/flx* mice expressing Cre in L2/3, L5, or L6 were similar across all layers. In particular, the eye dominance of units recorded from L2/3 were not different between *ngr1 flx/flx* mice and *ngr1 flx/flx; L2/3-Cre* mice (P = .40; KW test) (Figure. 2C), nor were units in L5 different between *ngr1 flx/flx* mice and *ngr1 flx/flx; L5-Cre* mice (P < .99; KW test) (Figure 2E). By comparison, the distribution of ODI scores in L2/3, L4, and L5 were all significantly shifted towards the non-deprived eye in *ngr1 flx/flx; L4-Cre* mice relative to *ngr1 flx/flx* controls (P < .008 for each comparison; KW test) (Figure 2D). Thus, loss of *ngr1* in L4 yields OD plasticity throughout V1 but does not promote cell-autonomous expression of OD plasticity when deleted in the surrounding layers.

However, recent studies have also identified some binocular neurons in the mouse LGN [40,41]. The *Scnn1a-Tg3-Cre* transgene we employed to delete *ngr1* in L4 also expresses Cre in the LGN [26,34]. Therefore, we examined two additional Cre drivers to determine if deleting *ngr1* in thalamus was sufficient to permit OD plasticity in adult mice: *nuclear receptor subfamily 5 group A (NR5a)-Cre*, a transgenic Cre driver line that also targets L4 [42], and *histidine decarboxylase (HDC)-Cre*, a ‘knock-in’ allele that directs Cre expression to LGN [43] (Figure 3 and Figure S3). We estimate that *NR5a-Cre* restricts Cre expression to approximately 30% of excitatory neurons in L4. Deleting *ngr1* in L4 with *NR5a-Cre* yielded OD plasticity following 4 days of MD, but deleting *ngr1* in LGN with *HDC-Cre* did not (4-day MD *ngr1 flx/flx, Nr5A-Cre* CBI = 0.48 ± .08, n = 4 vs. non-deprived *ngr1 flx/flx, Nr5A-Cre* CBI = 0.67 ± .02, n = 5, P = .039, and vs. 4-day MD *ngr1 flx/flx, HDC-Cre* CBI = 0.67 ± .04, n = 4, P = .022; KW test) (Figure 3C, D). The OD plasticity exhibited by adult *ngr1 flx/flx; Nr5A-Cre* was similar to that displayed by *ngr1 flx/flx; L2–6-Cre* and *ngr1 flx/flx; L4-Cre* mice. Thus, we confirmed that L4 gates OD plasticity through *ngr1*. A summary of this genetic dissection of the requirement for *ngr1* to limit OD plasticity is presented in Figure 3E.

Intracortical disinhibition but not thalamocortical disinhibition accompanies OD plasticity

To explore the circuit mechanisms in visual cortex associated with OD plasticity, we examined both intracortical disinhibition and thalamocortical disinhibition with electrophysiologic recordings from acute slices of V1 (Figure 4 and S4). Circuit mapping of synaptic inputs with laser-scanning photostimulation (LSPS) reveals the pattern of intracortical excitatory inputs onto PV inhibitory neurons in L2/3 (Figure 4A–C) [23,29]. MD for 1–2 days during the critical period promotes intracortical disinhibition by reducing excitatory synaptic drive onto PV interneurons [23,24]. This synaptic plasticity is confined to the critical period in WT mice, but is retained in adult *ngr1* −/− mice as well as *ngr1 flx/flx; PV-Cre* mice [19]. In adult *ngr1* −/− mice, 1–2 days of MD reduces the average excitatory synaptic input onto PV interneurons in L2/3 from neurons residing in L2/3, L4, and L5 [19]. To determine if 1 day of MD evoked similar disinhibition in adult *ngr1 flx/flx; L4-Cre* mice, we crossed this strain onto a second transgene that expresses GFP in PV interneurons in visual cortex, *GAD67-GFP* (Figure S4) [44]. Recorded cells were confirmed to exhibit the fast spiking activity with current injection that is characteristic of PV interneurons. The average excitatory synaptic current from neurons residing in L2/3 (P=.025), L4 (P=.036), and L5 (P <.001), was reduced significantly in *ngr1 flx/flx; L4-Cre* following 1–2 days of MD relative to non-deprived controls (two-way RM ANOVA with Sidak's multiple comparison test) (Figure 4E). Total synaptic current was also decreased significantly (Figure S4). Thus, adult *ngr1 flx/flx; L4-Cre; GAD67-GFP* mice exhibit intracortical disinhibition with 1–2 days of MD.

Synaptic plasticity at thalamocortical synapses has also been implicated as a mechanism contributing to OD plasticity in mouse. Anatomical studies measuring thalamocortical bouton size and number have proposed that thalamocortical synapses are reduced in juvenile mice by MD [45]. Thalamocortical synapse strength also increases in conditions promoting cross-modal plasticity within visual cortex in adult mice [46]. In contrast, one study has reported no change in the E/I ratio for thalamocortical inputs following 2–4 days of MD during the critical period [47]. These latter experiments employed optogenetic stimulation of thalamocortical axons transduced with an adeno-associated virus (AAV) to express a channelrhodopsin-2-enhanced yellow fluorescent protein (ChR2-YFP) in LGN.

To determine if disinhibition extends to thalamocortical synapses following 1 day of MD, we expressed ChR2-YFP extensively, but not exclusively, in LGN with *HDC-Cre* to direct expression of ChR2-YFP in heterozygous *CAG-COP4*H134R-EYFP (Ai32)* mice. We measured the E/I ratio of synaptic inputs onto L4 pyramidal neurons in juvenile (P26–30) WT mice with and without 1 day of MD by optogenetic stimulation of thalamocortical afferents in V1 at minimal power sufficient to evoke disynaptic inhibitory currents (Figure 5A, B and S5). We did not detect a significant change in the thalamocortical E/I ratio with MD (non-deprived, 1.1 ± 0.2, 16 cells; 1d MD, 0.7 ± .08, 20 cells, P = .15, MW test) (Figure 5C). Optogenetic stimulation of thalamocortical afferents in V1 near maximal intensity yielded similar results (Figure S5).

To determine if 1 day of MD did not alter the E/I ratio because of commensurate alterations to the strength of both excitatory thalamocortical inputs and disynaptic inhibitory inputs onto L4 neurons, we measured the amplitude of putative thalamocortical miniature

excitatory postsynaptic currents (mEPSCs) in this preparation as well [48]. We recorded Sr^{2+} desynchronized mEPSCs as described previously [46]. In the presence of 4 mM Sr^{2+}, stimulating ChR2 with a brief (5 ms) pulse of blue light evokes desynchronized synaptic release that yields a primary response followed by a brief train of mEPSCs (Figure 5D). The average amplitude of these evoked mEPSCs was nearly identical for L4 pyramidal neurons from P26–27 WT mice with and without 1 day of MD (non-deprived, 13 ± 1 pA, 14 cells; 1d MD, 14 ± 1 pA, 17 cells, P = .89, MW test) (Figure 5E). Consequently, we did not pursue thalamocortical disinhibition as a mechanism contributing to OD plasticity in combination with this genetic circuit dissection.

OD plasticity advances faster in L4 than L2/3 or L5 in mice

Last, we evaluated the progression of OD plasticity by layer. Electrophysiologic recordings in kittens has revealed that L2/3 and L5 display more rapid OD plasticity than L4 following brief MD [15]. The progression of OD plasticity by layer in mouse is less clear. Multi-unit electrophysiologic recordings to measure OD plasticity in mice indicate that 4 or more days are required to yield the maximal shift in eye dominance [5]. In contrast, a more recent study has reported that L2/3 and L4 display near complete OD plasticity simultaneously with 1 day of MD [16]. To discriminate between these disparate outcomes, we examined the effects of 2 days of MD in both juvenile WT mice (P26/27 at MD) and adult *ngr1 flx/flx; L4-cre* mice (P60–90 at MD) (Figure 6 and S6).

We identified a partial but significant reduction in CBI values for both groups following only 2d of MD (WT, non-deprived CBI = 0.76 ± .06, n = 6; 2d MD CBI = 0.61 ± .10, n = 7, P = .035; MW test; *ngr1 flx/flx, L4-Cre* non-deprived CBI = 0.71 ± .07, n =6; 2d MD CBI = 0.57 ± .11, n = 6, P = .041; MW test) (Figure S6). We evaluated cumulative distributions of the ODI scores for each cortical layer from these recordings. OD plasticity was more advanced after 2 days of MD in L4 than L2/3 or L5. The ODI scores from juvenile WT mice after 2 days of MD were significantly different from non-deprived mice in L4 but not in L2/3 or L5 (P<.0001, P=.19, and P=.48, respectively, KW test comparing all combinations of non-deprived, 2-day MD, and 4-day MD for each layer) (Figure 6A). Similarly, the ODI scores from adult *ngr1 flx/flx; L4-cre* mice after 2 days of MD were significantly different from the ODI scores from non-deprived mice in L4 but not in L2/3 or L5 (P<.0001, P=.06, and P=.11, respectively, KW test comparing all combinations of non-deprived, 2-day MD, and 4-day MD for each layer) (Figure 6B).

To determine the fraction of the overall OD shift following 4 days of MD that was present at 2 days of MD, we compared the medians of these cumulative distributions at 0, 2, and 4 days of MD for each layer and calculated the percentage of the overall change in ODI following 4 days MD present at 2 days of MD (Figure 6C). In juvenile WT mice, 2 days of MD attained nearly three-quarters of the overall OD shift measured following 4 days of MD in L4, but approximately half of the overall OD shift for L2/3 and L5. In adult *ngr1 flx/flx: L4-Cre* mice, 2 days of MD attained more than three-quarters of the overall OD shift measured following 4 days of MD in L4, but again approximately half of the overall OD shift for L2/3 and L5 (Figure 6C and Figure S6). We conclude from these experiments that OD plasticity advances faster in L4 than L2/3 or L5 in mice.

OD plasticity does not rely on a canonical cortical microcircuit

This finding that OD plasticity advances faster in L4 than L2/3 or L5 is consistent with a canonical circuit model for OD plasticity in which changes in eye dominance propagate from L4 to L2/3 to L5 [49]. A prediction of this model is that OD plasticity in L2/3 is required for OD plasticity in L5. To test this prediction, we employed pharmacology to attenuate OD plasticity in L2/3 during 4 days of MD and examined OD plasticity in L4 and L5 (Figure 7). AM-251 is a CB1 receptor antagonist that blocks OD plasticity in L2/3 during 1 day of MD [16]. We treated juvenile WT mice with AM-251 (5mg/kg) or vehicle (10% Tween 80, 20% dimethyl sulfoxide in water) as previously reported [16], but we repeated the dosing every 12 hours for 4 days in conjunction with MD.

Cumulative distributions of ODI values from L2/3 were significantly different between non-deprived mice and mice receiving 4 days of MD together with injection of vehicle solution (L2/3 non-deprived vs. L2/3 4D vehicle, P = .0002; KW test comparing non-deprived vs. 4-day MD with and without drug) (Figure 7A and Figure S7). However, treatment with AM-251 during MD abolished OD plasticity in L2/3 (L2/3 non-deprived vs. L2/3 4D AM-251, P> .99, KW test). In contrast, OD plasticity in both L4 and L5 were unaffected. In L4, the shift in OD following 4 days of MD was similar for mice treated with either drug or vehicle relative to non-deprived controls (L4 non-deprived vs. L4 4D vehicle, P = .01; L4 non-deprived vs. L4 4D AM-251 treated, P=.002; KW test comparing non-deprived vs. 4-day MD with and without drug) (Figure 7B). In L5, OD plasticity was likewise unaltered by drug treatment (L5 non-deprived vs. L5 4D vehicle, P = .01; L4 non-deprived vs. L4 4D AM-251 treated, P=.002; KW test comparing non-deprived vs. 4-day MD with and without drug) (Figure 7C). Thus, L5 does not inherit eye dominance from L2/3 nor require OD plasticity in L2/3.

Discussion

OD plasticity by adult *ngr1* mutant mice displays several hallmarks of OD plasticity otherwise confined to a developmental critical period [17]. Comparing the effects of MD on *ngr1* mutant mice relative to adult WT mice provides an opportunity to identify cortical circuit and signaling changes associated with OD plasticity outside the context of development when MD may have a number of effects on neural circuits, only some of which contribute to OD plasticity. For example, MD during the critical period not only alters eye dominance but also prevents the maturation of acuity by the deprived eye [50]. Previously we demonstrated that recovery of eye dominance and acuity following prolonged MD are independent in the mouse, and can be rescued separately by deleting *ngr1* either in cerebral cortex and thalamus, respectively [26].

To explore how OD plasticity is coordinated across cortical layers, we employed a genetic dissection strategy. We deleted *ngr1* in each cortical layer separately and evaluated the OD plasticity of neurons throughout V1. Deletion of *ngr1* in L2/3, L5, or L6, did not yield OD plasticity in adult mice. We did not detect cell-autonomous plasticity in the layer lacking *ngr1* or in any surrounding layer. In contrast, deletion of *ngr1* in L4 was sufficient to permit OD plasticity throughout V1 in adult mice. These experiments reveal that *ngr1* operates in L4 to confine OD plasticity to the critical period.

We then probed potential circuit mechanisms by which the deletion of *ngr1* in L4 neurons might sustain OD plasticity beyond the critical period. Several methods that enhance OD plasticity are predicted to increase the E/I ratio [14]. Environmental enrichment reduces the levels of GABA in visual cortex of rats to one-third the normal value as measured with microdialysis [51]. Similar findings have been reported for rats treated with fluoxetine [52]. Decreasing cortical inhibition by infusing inhibitors of either the GABA-A receptor, or of glutamic acid decarboxylases (GAD), an enzyme required for GABA synthesis, also enhances OD plasticity in rats [53]. However, the alterations within cortical circuitry induced by these interventions and reflected in these biochemical measurements have not been determined.

Circuit mapping with LSPS in acute slices from WT mice has revealed that 1–2 days of MD during the critical period promotes disinhibition mediated by a reduction of intracortical excitatory input onto PV interneurons in V1 [23]. This disinhibition in response to MD is confined to the critical period [19,23]. Interestingly, mimicking disinhibition by reducing activity of cortical PV interneurons with the expression of inhibitory designer receptors exclusively activated by designer drugs (DREADDS) and administration of the ligand clozapine-n-oxide appears sufficient to reinstate OD plasticity as measured with calcium imaging 'optical field potentials' [23]. Adult *ngr1 −/−* mutants and *ngr1 flx/flx; PV-Cre* mice retain the capacity for both disinhibition and OD plasticity [19]. Intracortical disinhibition accompanied OD plasticity in *ngr1 flx/flx; L4-Cre* mice as well. We conclude that L4 confines disinhibition associated with OD plasticity to the critical period.

L4 is well positioned to gate intracortical disinhibition across cortical layers. Excitatory neurons residing in L4 of visual cortex provide substantial synaptic input to neurons in L2/3, L4, and L5 [29]. In fact, interlaminar synapses from L4 onto L2/3 and L5 neurons are stronger than the intralaminar synapses between L4 neurons. By comparison, inhibitory synaptic inputs are predominantly intralaminar [29]. In our LSPS experiments, 1–2 days of MD in mice lacking *ngr1* in L4 reduced excitatory synaptic input onto PV interneurons from excitatory neurons in L2/3, L4, and L5. This finding supports a model for disinhibition following MD in which L4 affects cortical inputs to PV interneurons from not only L4 but also the surrounding layers. To determine if disinhibition extended to thalamocortical inputs, we investigated the strength of these synapses with optogenetics.

Thalamocortical disinhibition is proposed to contribute to OD plasticity [54]. Adult mice lacking expression of SynCAM-1 possess OD plasticity as measured with visually-evoked potentials. In these mutant mice the strength of thalamocortical synapses onto PV interneurons are reduced as inferred from immunohistochemical staining to quantify the number of puncta with vesicular glutamate transporter 2 (Vglut2) signal. Fewer and smaller presumptive thalamocortical synapses have also been observed in juvenile WT mice receiving MD with electron microscopy by immunolabeling with antibodies directed against Vglut2 [55]. In contrast to these histochemical approaches for evaluating the strength of thalamocortical synapses, we employed optogenetic stimulation of thalamocortical afferents to determine if the relative E/I ratio and/or strength of thalamocortical mEPSCs onto L4 pyramidal neurons in V1 was altered in WT mice by 1 day of MD during the critical period

[46]. We did not detect any change in the thalamocortical E/I ratio or average mEPSC amplitude.

Our findings are consistent with a published study examining the effects of 2–4 days of MD using a similar technique [47]. This preceding study also reported a small decrease (~10%) in the strength of mEPSCs evoked by optogenetic stimulation in the presence of tetrodotoxin. By comparison, we did not observe any reduction in the amplitude of mEPSCs evoked by optogenetic stimulation and desynchronized with strontium [46]. The amplitudes of the evoked excitatory responses were consistently larger in our recordings, perhaps as a consequence of the more extensive expression of ChR2-YFP in thalamus directed by the *HDC-Cre* relative to ChR2-YFP expression achieved by transduction with AAV. Overall, we conclude from these slice electrophysiology experiments that intracortical disinhibition is a principal component of OD plasticity, while the role of thalamocortical disinhibition and/or reduced synaptic strength of thalamic inputs onto L4 pyramidal neurons is less important.

How NgR1 might function to limit disinhibition and OD plasticity remains unclear. One study has reported that cortical pyramidal neurons in *ngr1* −/− mice exhibit dramatically increased spine turnover [56]. A central prediction of that study was that NgR1 regulates experience-dependent cortical plasticity in a cell-autonomous manner by restricting the rate of synaptic structural plasticity [56]. We are unable to reproduce the result that *ngr1* −/− mice display elevated spine turnover although we performed *in vivo* two-photon imaging experiments nearly identical in design. Our measurements of spine turnover in *ngr1* −/− mice were identical to WT controls [57]. Nonetheless, here we tested the prediction that deletion of *ngr1* in excitatory neurons in L2/3 or L5 would yield cell-autonomous OD plasticity. We conclude that loss of *ngr1* in cortical neurons L2/3 or L5 is not sufficient to promote OD plasticity in a cell-autonomous manner.

There is little precedent to provide context for the finding that L4 confines OD plasticity to the critical period across cortical layers. We propose that L4 gates OD plasticity by restricting disinhibition following MD. Cortical disinhibition is associated with a reduction in the amplitudes but not the frequency of mEPSCs in PV interneurons [23], and requires a decrease in signaling by the ErbB4 tyrosine kinase receptor in PV interneurons [24]. Perhaps the strength of intracortical excitatory synapses onto PV interneurons decreases with 1 day of MD because the receptor content of these synapses relies on a threshold level of cellular ErbB4 activity to which thalamocortical synapses are insensitive. Loss of NgR1 by L4 neurons may permit MD to attenuate ErbB4 signaling in adult PV interneurons, thereby decreasing the strength of intracortical excitatory synapses from both L4 and the surrounding layers onto these inhibitory neurons. However, the mechanism by which NgR1 may influence ErbB4 signaling is unclear, as NgR1 activates a distinct signaling pathway involving rho-associated protein kinase 1 downstream of the RhoA GTPase [58].

How OD plasticity emerges and propagates through cortical circuitry has proven difficult to resolve. Some of the earliest work testing the effects of very brief durations of MD (4–8 hours) on binocularity in kitten visual cortex concluded that OD plasticity occurs first in L4 and L5 [59]. In contrast, a subsequent study examining the effects of 1 day of MD in kittens proposed that OD plasticity advances faster in L2/3, L5, and L6, than L4 [15]. Yet these

experiments were not identical in design. the latter study targeted recordings to the junction of eye dominance domains rather than probing uniformly across V1.

In the mouse, OD plasticity has been reported to be simultaneous but independent in L2/3 and L4 [16]. However, the OD plasticity in this study was unusually fast, resulting in near complete shifts in eye dominance following a single day of MD for both L2/3 and L4. In addition, these experiments employed custom-designed electrodes and an unconventional analysis method. Such rapid shifts in OD are not evident in numerous other studies [5,10,11], nor in our recordings where we observe that OD plasticity advanced more rapidly in L4 than L2/3 or L5 (Figure 6). This difference seems unlikely to be a consequence of sampling bias in our experiments because we examined a similar number of mice (7 vs. 9) and more units (133 vs. 50) [16].

OD plasticity advancing more rapidly in L4 than other layers is consistent with it propagating through a canonical cortical microcircuit. To test whether OD plasticity follows this classic circuit, we employed pharmacology to prevent OD plasticity in L2/3 and examined the consequences on L5. AM-251 is a potent antagonist for the cannabinoid receptor CB1 with a Ki near 8 nanomolar [60]. A single injection is sufficient to block OD plasticity in L2/3 during one day of MD [16]. In acute slices, bath application of AM-251 also impairs long-term depression (LTD) in L2/3 of V1, albeit at concentrations 250 times greater than the Ki (2 micromolar vs. 8 nanomolar) [61]. Twice daily injections of AM-251 prevented OD plasticity in L2/3 during 4 days of MD. However, this treatment had no detectable effect on OD plasticity in L5. Thus, OD plasticity in L5 does not require corresponding plasticity in L2/3. This finding is not consistent with OD plasticity relying on a canonical cortical microcircuit. We propose that L2/3 and L5 operate more independently than expected from the canonical circuit model.

Recent work has identified that some thalamic neurons receive binocular input and display OD plasticity [40,41,62]. One calcium imaging study estimated that 15% of LGN neurons are binocular in the adult mouse [41]. A second study similar in design reported 6% of neurons have binocular responses [63]. However, multi-unit recordings from linear electrode arrays positioned in LGN reveal that OD shifts in V1 are largely not inherited from thalamus [40]. Our experiments do not discriminate whether the OD shifts we observe in L4 with 2 days of MD in WT mice are a result of OD plasticity by L4 neurons, or a consequence of plasticity within LGN that is then inherited by L4, or some combination thereof. But given that deletion of *ngr1* in L4 but not LGN is sufficient to permit OD plasticity in adult mice, we favor the model that L4 gates OD plasticity. Likewise, the thalamocortical, intracortical, and callosal contributions to OD plasticity in L2/3 and L5 are as yet unclear [64]. Future work will be required to investigate these possible circuit mechanisms for experience-dependent visual plasticity.

The mouse has limitations for understanding visual system circuitry but has proven a useful model for investigating tuning characteristics of neurons in visual cortex that conserved with other mammals [65], as well as experience-dependent plasticity [66]. Here we have exploited genetic resources for the mouse in combination with electrophysiology and circuit manipulations to probe how experience-dependent plasticity is coordinated within the

laminar circuitry of V1. We conclude from these experiments that L4 regulates intracortical disinhibition to gate OD plasticity in visual cortex and that OD plasticity advances faster in L4 than L2/3 or L5 but does not rely on a canonical cortical microcircuit for expression.

STAR Methods

RESOURCE AVAILABILITY

Lead Contact—Aaron W. McGee (aaron.mcgee@louisville.edu)

Materials Availability—Further information and requests for resources and reagents should be directed to and will be fulfilled by the lead contact. Requests for mouse strains developed by third parties will be directed to the appropriate contact. This study did not generate unique reagents.

Data and Code Availability—This study did not generate code.

Primary data has been deposited in Mendeley Data:

https://data.mendeley.com/datasets/2xz34tkxmf/draft?a=1583d81c-4d4d-418d-8337–2ef331ba127b

EXPERIMENTAL MODEL AND SUBJECT DETAILS

Mice—The lead contact designed and validated the *ngr1 flx* allele [25]. Both the constitutive *ngr1 (−/−)* and conditional *ngr1 flx/flx* mouse strains have been characterized [25,67]. These strains had been repeatedly backcrossed onto the C57Bl6J background to at least F8. Subsequently, the *ngr1flx/flx* line was backcrossed against C57Bl6J with either the *CamK2a-Cre (L2–6-Cre)*, *Scnn1a-Cre (L4-Cre), Nr5a-Cre, Rpb4a-Cre (L5-Cre)*, *Ntsr1-Cre (L6-Cre)*, or *HDC-Cre* driver lines [28,34–36,42,43]. The *CamK2a-Cre*, *Scnn1a-Cre*, *Nr5a-Cre*, and *HDC-Cre* driver strains were imported from Jackson Labs (strain numbers 005359, 009613, 012462, and 021198, respectively). The *Rbp4a-Cre* and *Ntsr1-Cre* strains were imported from the Mutant Mouse Resource and Research Center (MMRRC) (031125-UCD and 030648-UCD). Wildtype mice are C57Bl6J (The Jackson Laboratory, strain 00664). The specificity for each Cre driver line was validated by crossing each line to the Cre reported line *Ai14* (tdTomato) (The Jackson Laboratory, strain 007914). For LSPS circuit mapping experiments, *ngr1 flx/flx; Scnn1a-Cre* mice were crossed onto the background *Tg(Gad1-EGFP)G42Zjh/J* (Jackson Laboratory strain number 077677) [44]. For slice electrophysiology experiments, HDC-Cre mice were crossed against *B6.Cg-Gt(ROSA)26Sortm32(CAG-COP4*H134R/EYFP)Hze/J (Ai32)* homozygous mice (Jackson Laboratory strain number 024109). Experiments and procedures were performed on both adult male and female mice by an experimenter blind to genotype and/or treatment condition. Mice were group housed and maintained on a 12-hr light/dark cycle under standard housing conditions. For experimental and control groups including the *ngr1 flx/flx* line, experiments were performed on littermates. Genotyping was performed using custom primer sets for polymerase chain reaction (PCR) amplification with REDExtract-N-Amp PCR kit (XNAT, Sigma). All mice were genotyped for germline recombination of the *ngr1*

flx allele with custom primer sets. Mice with germline recombination were ejected from the study.

All procedures and care were performed in accordance with the guidelines of the Institutional Animal Care and Use Committees at Children's Hospital Los Angeles, the University of California, Irvine, and the University of Louisville.

METHOD DETAILS

Monocular Deprivation (MD)

One eye was closed on postnatal day 25–27, or P60–90 using a single mattress suture tied with 6–0 polypropylene monofilament (Prolene 8709H; Ethicon) under brief isoflurane anesthesia (2%) for durations described. The knot was sealed with cyanoacrylate glue. Upon removing the suture, the eye was examined under a stereomicroscope and animals with scarring of the cornea were eliminated from the study.

Electrophysiological Recordings in Visual Cortex

Recordings and analysis were performed blind to genotype or drug treatment. Methods were adapted from previously published methods [26]. In brief, mice were anesthetized with isoflurane (4% induction, 1–2% maintenance in O_2 during surgery). The mouse was placed in a stereotaxic frame and body temperature was maintained at 37°C by a homeostatically-regulated heat pad (TCAT-2LV, Physitemp). Dexamethasone (4 mg/kg s.c.; American Reagent) was administered to reduce cerebral edema. The eyes were flushed with saline and the corneas were protected thereafter by covering the eyes throughout the surgical procedure with ophthalmic ointment (Puralube, Dechra Pharmaceuticals), and with frequent application of saline. A craniotomy was made over visual cortex in the left hemisphere and a custom-designed aluminum head bar was attached with cyanoacrylate glue or Metabond over the right hemisphere to immobilize the animal during recording. Prior to transfer to the recording setup, a dose of chlorprothixene (0.5 mg/kg i.p.; C1761, Sigma) was administered to decrease the level of isoflurane required to maintain anesthesia to 0.6%.

Recordings were made with Epoxylite-coated tungsten microelectrodes with tip resistances of 10–15 MΩ (FHC). The signal was amplified (model 3600; A-M Systems), low-pass filtered at 3000Hz, high-pass filtered at 300Hz, and digitized (micro1401; Cambridge Electronic Design). Multi-unit activity was recorded from four to six locations separated by >90μm in depth for each electrode penetration. In each mouse, there were four to six penetrations separated by at least 200μm across the binocular region of primary visual cortex, defined by a receptive field azimuth < 25°. Responses were driven by drifting sinusoidal gratings (0.1cpd, 95% contrast), presented in six orientations separated by 30° (custom software, MATLAB). The gratings were presented for 2s of each 4s trial. The grating was presented in each orientation in a pseudorandom order at least four times, interleaved randomly by a blank, which preceded each orientation once. Action potentials (APs) were identified in recorded traces with Spike2 (Cambridge Electronic Design). Only waveforms extending beyond 4 standard deviations above the average noise were included in subsequent analysis. For each unit, the number of APs in response to the grating stimuli was

summed and averaged over the number of presentations. If the average number of APs for the grating stimuli was not greater than 50% above the blank, the unit was discarded. Units were classified as L2/3, L4, or L5 according to recording depth of the electrode measured from the pial surface. Units recorded between 150–300 microns were classified at L2/3, between 350–450 microns as L4, and between 500–700 microns as L5 [29].

The ocular dominance index (ODI) was calculated for each unit by comparing the number of APs elicited in a given unit when showing the same visual stimulus to each eye independently. Units were assigned to one of seven OD categories (1–7) where units assigned to category 1 are largely dominated by input from the contralateral eye, and units assigned to category 7 are largely dominated by input from the ipsilateral eye [1]. To categorize each unit, the average number of APs elicited by the blank was subtracted from the average number of APs elicited by the gratings for the contralateral eye (CE) and the ipsilateral eye (IE). Next, the ocular dominance index (ODI), given by ODI = (IE - CE)/(IE + CE) was calculated for each unit and assigned to OD categories 1–7 as follows: −1 to −0.6 = 1, −0.6 to −0.4 = 2, −0.4 to −0.1 = 3, −0.1 to 0.1 = 4, 0.1 to 0.4 = 5, 0.4 to 0.6 = 6, 0.6 to 1 = 7. Finally, the sum of the number of cells in each category was used to calculate the CBI for each animal with the formula: CBI = [(n1 – n7) + (2/3)(n2 – n6) + (1/3)(n3 – n5) + N]/2N where N is the total number of units and nx is the number of units with OD scores equal to × [5].

Immunohistochemistry

Mice were deeply anesthetized with Ketamine HCl (200mg/kg, Phoenix pharmaceuticals)/ Xylazine (20mg/kg, Lloyd Laboratories) and perfused transcardially with phosphate-buffered saline (PBS; ChemCruz SC-362299) followed by a buffered 4% paraformaldehyde (PFA)/PBS (Acros Organics 416780030). Brains were removed and post-fixed overnight in 4% PFA/PBS. Free-floating 50μm sections were cut on a vibrating microtome (Leica VT 1000S) while submerged in PBS and preserved in PBS containing 0.05% sodium azide (Sigma-Aldrich S8032).

Coronal sections containing visual cortex and LGN were washed in PBS (3 × 5 minutes) and incubated in blocking solution, 3% normal donkey serum (NDS; Jackson ImmunoResearch) in PBS containing 0.1% Triton X-100 (Sigma-Aldrich T9284) (PBS-T) for 1 h at room temperature. The primary antibodies rabbit anti-GFP (Novus, NB600–308) or sheep anti-PV (R&D Systems. AF5058) were diluted in blocking solution to 1μg/ml and sections incubated in primary antibody overnight at 4°C. After repeated washing in PBS-T (3 × 10 min), sections were incubated in Alexa 488-conjugated secondary antibody (Jackson ImmunoResearch, 1:200 in blocking solution) overnight at 4°C. Thereafter sections were washed 3 × 10 min in PBS-T and mounted onto SuperFrost Plus slides (Fisher) with Fluoromount G containing DAPI (Southern Biotech). Images of the entire hemisphere containing V1 and LGN were captured using an Olympus BX51 stereoscope with a 12-bit monochrome camera (Retiga, Q Imaging) through a 10X PLAN 0.25 NA lens (Olympus). High magnification images of V1 and LGN from coronal sections stained with anti-GFP were captured with a 20X PLAN 0.4 NA objective (Olympus). DAPI staining was utilized to

demarcate visual cortex and LGN. All images received only linear contrast adjustment and cropping with imaging software (Photoshop, Adobe).

In utero electroporation (IUEP)

pCAG:Cre-GFP was a gift from Connie Cepko (Addgene plasmid # 13776) [32]. Mating pairs of *ngr1 flx/flx* mice were set up for a single night and separated the following morning. Pups of gravid females underwent the procedure on E15.5 [68]. In brief, anesthesia was induced with 4% isoflurane and maintained with 1.5%. A glass pipette (Tritech Research) was backfilled with a pCAG:Cre-GFP plasmid (concentration 0.5–1 μg/μl). Pups were removed one wing at a time and kept moist and warm with sterile saline. The left lateral ventricle was injected with 0.5–1 μg of plasmid. Electroporation was performed with a square-wave electroporator (CUY21 SC, Nepagene) using a 3-electrode configuration to target occipital cortex [33]. Following electrophysiological recordings in visual cortex, transfection of plasmid into L2/3 neurons was confirmed by immunohistochemistry. Mice in which expression of GFP was not expressed in at least 30% of neurons in L2/3 were not included in the analysis.

Laser scanning photostimulation for circuit mapping

Electrophysiological recordings and photostimulation were performed as described [69]. Electrophysiological data were acquired with a Multiclamp 700B amplifier (Molecular Devices), data acquisition boards (models PCI MIO16E-4 and 6713, National Instruments) and custom-modified version of Ephus software [70]. Data were digitized at 10 kHz.

The laser scanning photostimulation (LSPS) procedures were similar to those described previously [23,71]. LSPS was performed through a 4X objective lens. Stock solution of MNI-caged-L-glutamate (Tocris Bioscience) was added to 20 ml ACSF for a concentration of 0.2mM caged glutamate. The cortical slice image, acquired through the 4X objective, was visualized using a high-resolution digital CCD camera, and this image was used to guide and register photostimulation sites. An electro-optical modulator and a mechanical shutter controlled the delivery of 1.5-millisecond duration, 15-mW pulses from a 350nm UV laser (DPSS Lasers) to the slice. Focal laser spots approximated a Gaussian profile with a lateral width of 50–100 μm. Under our experimental conditions, LSPS-evoked action potentials were recorded from stimulation locations within 100 μm of targeted excitatory neuronal somata and occurred within 150 ms after photostimulation. This indicates that LSPS has a sufficient resolution for V1 laminar circuit mapping. LSPS-evoked EPSCs in patched neurons were detected under voltage clamp at an empirically determined membrane potential of −70mV. By systematically surveying synaptic inputs from hundreds of different sites across a large cortical region, aggregate synaptic input maps were generated for individual neurons. For our mapping experiments, a standard stimulus grid (16 X 16 stimulation sites, 65 μm^2 spacing) was used to tessellate V1 from pia to white matter. The LSPS site spacing was empirically determined to capture the smallest predicted distance in which photostimulation differentially activates adjacent neurons. Glutamate uncaging was delivered sequentially in a non-raster, non-random sequence, following a ‘shifting-X’ pattern designed to avoid revisiting the vicinity of recently stimulated sites [72].

Laminar circuit input analysis

Photostimulation induces two forms of excitatory responses: (1) those that result from direct activation of the recorded neuron's glutamate receptors; and (2) synaptic responses (EPSCs) resulting from the suprathreshold activation of presynaptic excitatory neurons. Responses that occur within 10 ms of laser pulse onset were considered direct; these responses exhibited a distinct shape and occurred immediately after glutamate uncaging. Synaptic currents with such short latencies are not possible because they would have to occur before the generation of action potentials in photostimulated neurons. Therefore, direct responses need to be excluded from local synaptic input analysis. At some locations, synaptic responses were over-riding on relatively small direct responses; such responses were identified and included in synaptic input analysis as described previously [23]. To check for any systematic differences across treatment conditions, the spatial extent and frequency of action potentials elicited in response to direct photostimulation were determined in a subset of the experiments by performing whole-cell recordings in current-clamp mode using an 8 X 8 mapping grid. Photostimulation excitation profiles assessed by glutamate uncaging were found to be similar for control and MD.

For data map analysis, LSPS-evoked EPSCs were quantified across the 16 X 16 mapping grid for each cell, and 2 to 4 individual maps were averaged per recorded cell, reducing the likelihood of incorporating noise events in the analysis window (150 ms). Averaged maps were then analyzed using the 4X DIC image to bin responses according to laminar cytoarchitectonic landmarks. Synaptic events were binned from locations spanning ±195 μm tangential to the targeted soma location and from the top of layer 2/3 to the bottom of layer 6 across the radial vector. Data were plotted as the average integrated EPSC amplitude per map location.

Optogenetic evoked E/I ratio

HDC-Cre × *Ai32* mice (P26–30; male and female) were anesthetized deeply with isoflurane vapors (4 %) before being rapidly decapitated. The brain was removed and placed for 2 minutes in 4° C oxygenated (95% O_2/5% CO_2) cutting buffer containing (in mM): Sucrose 234, glucose 11, KCl 2.5, $MgSO_4$ 10, $CaCl_2$ 0.5, $NaHCO_3$ 26, and NaH_2PO_4 1.25. A vibratome (Leica VT1200S) was used to make 270 μm-thick coronal slices containing visual cortex. Slices were incubated for 30 minutes in 32° C oxygenated artificial cerebrospinal fluid (ACSF) containing (in mM): NaCl 126, $NaHCO_3$ 26, glucose 10, KCl 2.5, $MgCl_2$ 2, $CaCl_2$ 2, & NaH_2PO_4 1.25. After incubation, slices were maintained in ACSF at room temperature.

An upright microscope (Olympus BX51WI), equipped with DIC optics and a CCD camera (Olympus Y-150), was used to visualize the slice through 10x and 60x objectives (Olympus). To photoactivate of ChR2-containing thalamocortical (TC) afferents, a light-emitting diode (LED; Prizmatix) was used to deliver blue light (peak wavelength 460nm) through the 60x water-immersion objective. Borosilicate glass patch electrodes were pulled using a vertical pipette puller (Narashige PC-10). Recording pipettes had tip resistances of 5–7 MΩ. Data were acquired using Multiclamp 700B amplifier (Molecular Devices), filtered at 3–10 kHz, and digitized using Digidata 1440A (Molecular Devices). For MD experiments, recordings

were performed from visually-identified pyramidal neurons in layer 4 of the left primary visual cortex, contralateral to the deprived eye. In controls, cells were recording from both hemispheres. Pipette and whole-cell capacitances were monitored and compensated for during recordings. Input resistance (R_i) and access resistance (R_a) were monitored throughout the experiment by periodically applying brief hyperpolarizing voltage steps. Neurons were held in voltage-clamp mode at V_H= −60 mV for at least 5 minutes after achieving whole-cell configuration before data acquisition. Neurons with R_i < 150 were excluded from analysis. In addition, neurons with R_a > 25, or >20% change in R_a were excluded from analysis. To measure E/I ratio, slices were transferred to a recording chamber containing 32° C oxygenated ACSF and continuously perfused at 2–3 ml/min. To reduce multi-synaptic activity, 1 μM 2-chloroadenosine was added to ACSF. The internal recording solution contained (in mM): Cs-gluconate 117, CsCl 13, CsOH 117, $CaCl_2$ 0.7, $MgCl_2$ 1, EGTA 0.1, HEPES 10, Na-ATP 2, Na-GTP 0.4, QX-314 5 (pH 7.3, 290 mOsm). TC-evoked monosynaptic excitatory postsynaptic currents (EPSCs) and disynaptic inhibitory postsynaptic currents (IPSCs) were recorded in voltage clamp mode, holding at −50 mV or 5 mV, respectively. LED light (single 5ms pulse) intensity was set to a minimum power needed to reliably evoke an IPSC with a single peak. For the same neurons, responses maximal intensity LED stimulation were also recorded. Within each neuron, EPSCs and IPSCs were recorded with the same LED power intensity. At least 5 repetitions were made at each holding potential, with a 15-second interval between pulses. A coin flip was used to determine whether the EPSC or IPSC was recorded first. ClampFit software (Molecular Devices) was used to measure the peak amplitude of EPSCs (11–16 ms. post stimulus onset) and IPSCs (13–20 ms. post stimulus onset). A 200 ms. period immediately preceding the onset of LED stimulus was used as the baseline. Neurons with average absolute EPSC or IPSC amplitude of less than 50 pA were excluded from analysis. Only 2 cells were excluded in total. To determine the E/I ratio for each neuron, average EPSC peak amplitude was divided by average IPSC amplitude.

Optogenetic evoked desychronized synaptic events

Acute brain slices containing visual cortex were prepared as described above. To measure mEPSCs, slices were transferred to a recording chamber perfused with oxygenated Ca^{2+}-free, strontium-modified ACSF maintained at 32° C and containing (in mM): NaCl 126, $NaHCO_3$ 26, glucose 10, KCl 2.5, $MgCl_2$ 4, $SrCl_2$ 4, & NaH_2PO_4 1.25. Pharmacological blockers SR 95531 (10 μM) and (RS)-CPP (10 μM) were included in the recording ACSF to block $GABA_A$ and NDMA receptors, respectively. Each slice was incubated in the recording chamber for at least 15 minutes before the start of recordings. The internal solution contained (in mM): Cs-gluconate 117, CsCl 13, CsOH 117, $MgCl_2$ 1, EGTA 0.3, HEPES 10, TEA-Cl 10, Na-ATP 2, Na-GTP 0.4, QX-314 5 (pH 7.3, 290 mOsm). Recordings were made in voltage-clamp mode, with neurons held at −80 mV. A single 5 ms blue light pulse was used to photoactivate TC afferents and evoke a reliable EPSC, followed by Sr^{2+}-desynchronized miniature EPSCs. At least 50 repetitions were conducted for each neuron, with an interstimulus interval of 10 seconds. MiniAnalysis software (Synaptosoft) was used to detect and measure the amplitude of Sr^{2+}-desynchronized mEPSCs. Events occurring between 50–450 ms after stimulus onset with amplitude > 3× root mean square (RMS) noise

were included in the analysis. Events with amplitudes > 30pA were excluded from analysis. Neurons with RMS noise > 3.5, or less than 50 total events were excluded from analysis.

Biocytin and nuclear staining

Biocytin (0.1 – 0.2% w/v; Sigma) was included in the internal solution to allow for labeling of recorded neurons in all whole-cell electrophysiology experiments. After completion of recordings, slices were post-fixed overnight in 4% PFA. Sections were then washed for 20 minutes in PBS and incubated overnight in Streptavidin Alexa Fluor 647 and 1% Triton X-100. The next day, the sections were washed, incubated for 10 minutes in Hoechst 33342 (1:2000), washed again and mounted on glass slides with Fluoromount G (Southern Biotech). Only layer 4 pyramidal V1 neurons were included in the analysis, with the identity of each neuron being confirmed by soma location and presence of an apical dendrite.

AM-251 Treatment

AM-251 was administered as previously described [16]. In brief, AM-251 (Tocris, 1117) was solubilized in a vehicle solution containing 10% Tween-80 (Sigma, P1754) and 20% dimethyl sulfoxide (Sigma, 41640) at 2 mg/ml. The drug solution was formulated each day. Groups of juvenile WT mice were treated twice daily by intraperitoneal injection at 5 mg/kg for 4 consecutive days starting at P26 with either drug or a corresponding volume of vehicle solution. The first injection was concomitant with monocular deprivation.

Quantification and Statistical Analysis

All statistical analyses were performed using Prism software (version 8.0, GraphPad). Group numbers are stated in the Results and Figure Legends. *N* represents the number of mice for group comparisons and units for cumulative distributions, except for Figures 4 and 5 where *n* corresponds to the number of cells. Unless otherwise stated, group comparisons were made using the Kruskal-Wallis test with Dunn's correction. The specific pairwise tests are described in the Results section. Values presented are the mean plus/minus the standard deviation.

Supplementary Material

Refer to Web version on PubMed Central for supplementary material.

Acknowledgments

This research is supported by the National Eye Institute (R01EY021580, R01EY027407, and R01EY028212).

References

1. Wiesel TN, and Hubel DH (1963). Single-Cell Responses in Striate Cortex of Kittens Deprived of Vision in One Eye. J. Neurophysiol 26, 1003–1017. [PubMed: 14084161]
2. Hubel DH, Wiesel TN, and LeVay S. (1977). Plasticity of ocular dominance columns in monkey striate cortex. Philos. Trans. R. Soc. Lond. B. Biol. Sci 278, 377–409. [PubMed: 19791]
3. Drager UC (1978). Observations on monocular deprivation in mice. J. Neurophysiol 41, 28–42. [PubMed: 621544]

4. Fagiolini M, Pizzorusso T, Berardi N, Domenici L, and Maffei L. (1994). Functional postnatal development of the rat primary visual cortex and the role of visual experience: Dark rearing and monocular deprivation. Vision Res. 34, 709–720. [PubMed: 8160387]
5. Gordon JA, and Stryker MP (1996). Experience-dependent plasticity of binocular responses in the primary visual cortex of the mouse. J. Neurosci 16, 3274–3286. [PubMed: 8627365]
6. Antonini A, Fagiolini M, and Stryker MP (1999). Anatomical correlates of functional plasticity in mouse visual cortex. J. Neurosci 19, 4388–4406. [PubMed: 10341241]
7. Oray S, Majewska A, and Sur M. (2004). Dendritic Spine Dynamics Are Regulated by Monocular Deprivation and Extracellular Matrix Degradation. Neuron 44, 1021–1030. [PubMed: 15603744]
8. Mataga N, Mizuguchi Y, and Hensch TK (2004). Experience-dependent pruning of dendritic spines in visual cortex by tissue plasminogen activator. Neuron 44, 1031–1041. [PubMed: 15603745]
9. Malenka RC, and Bear MF (2004). LTP and LTD: An embarrassment of riches. Neuron 44, 5–21. [PubMed: 15450156]
10. Frenkel MY, and Bear MF (2004). How monocular deprivation shifts ocular dominance in visual cortex of young mice. Neuron 44, 917–923. [PubMed: 15603735]
11. Sato M, and Stryker MP (2008). Distinctive features of adult ocular dominance plasticity. J. Neurosci 28, 10278–10286. [PubMed: 18842887]
12. Pham TA, Graham SJ, Suzuki S, Barco A, Kandel ER, Gordon B, and Lickey ME (2004). A semi-persistent adult ocular dominance plasticity in visual cortex is stabilized by activated CREB. Learn. Mem 11, 738–747. [PubMed: 15537732]
13. Morishita H, and Hensch TK (2008). Critical period revisited: impact on vision. Curr. Opin. Neurobiol 18, 101–107. [PubMed: 18534841]
14. Levelt CN, and Hübener M. (2012). Critical-Period Plasticity in the Visual Cortex. Annu. Rev. Neurosci 35, 309–330. [PubMed: 22462544]
15. Trachtenberg JT, Trepel C, and Stryker MP (2000). Rapid extragranular plasticity in the absence of thalamocortical plasticity in the developing primary visual cortex. Science 287, 2029–2032. [PubMed: 10720332]
16. Liu C-H, Heynen AJ, Shuler MGH, and Bear MF (2008). Cannabinoid Receptor Blockade Reveals Parallel Plasticity Mechanisms in Different Layers of Mouse Visual Cortex. Neuron 58, 340–345. [PubMed: 18466745]
17. Stephany CÉC-E, Frantz MGMG, and McGee AWAW (2016). Multiple Roles for Nogo Receptor 1 in Visual System Plasticity. Neuroscientist 22, 653–666. [PubMed: 26552866]
18. Baldwin KT, and Giger RJ (2015). Insights into the physiological role of CNS regeneration inhibitors. Front. Mol. Neurosci 8, 1–8. [PubMed: 25674046]
19. Stephany C-É, Ikrar T, Nguyen C, Xu X, and McGee AW (2016). Nogo receptor 1 confines a disinhibitory microcircuit to the critical period in visual cortex. J. Neurosci 36.
20. McGee AW, Yang Y, Fischer QS, Daw NW, and Strittmatter SH (2005). Neuroscience: Experience-driven plasticity of visual cortex limited by myelin and nogo receptor. Science 309, 2222–2226. [PubMed: 16195464]
21. Stephany CÉ, Chan LLH, Parivash SN, Dorton HM, Piechowicz M, Qiu S, and McGee AW (2014). Plasticity of binocularity and visual acuity are differentially limited by nogo receptor. J. Neurosci 34, 11631–11640. [PubMed: 25164659]
22. Hensch TK, Fagiolini M, Mataga N, Stryker MP, Baekkeskov S, and Kash SF (1998). Local GABA circuit control of experience-dependent plasticity in developing visual cortex. Science 282, 1504–1508. [PubMed: 9822384]
23. Kuhlman SJ, Olivas ND, Tring E, Ikrar T, Xu X, and Trachtenberg JT (2013). A disinhibitory microcircuit initiates critical-period plasticity in the visual cortex. Nature 501, 543–546. [PubMed: 23975100]
24. Sun Y, Ikrar T, Davis MF, Gong N, Zheng X, Luo ZD, Lai C, Mei L, Holmes TC, Gandhi SP, et al. (2016). Neuregulin-1/ErbB4 Signaling Regulates Visual Cortical Plasticity. Neuron 92, 160–173. [PubMed: 27641496]
25. Wang X, Duffy P, McGee AW, Hasan O, Gould G, Tu N, Harel NY, Huang Y, Carson RE, Weinzimmer D, et al. (2011). Recovery from chronic spinal cord contusion after nogo receptor intervention. Ann. Neurol 70, 805–821. [PubMed: 22162062]

26. Stephany CÉ, Ma X, Dorton HM, Wu J, Solomon AM, Frantz MG, Qiu S, and McGee AW (2018). Distinct Circuits for Recovery of Eye Dominance and Acuity in Murine Amblyopia. Curr. Biol 28, 1914–1923. [PubMed: 29887305]
27. Dräger UC (1975). Receptive fields of single cells and topography in mouse visual cortex. J. Comp. Neurol 160, 269–289. [PubMed: 1112925]
28. Tsien JZ, Chen DF, Gerber D, Tom C, Mercer EH, Anderson DJ, Mayford M, Kandel ER, and Tonegawa S. (1996). Subregion- and cell type-restricted gene knockout in mouse brain. Cell 87, 1317–1326. [PubMed: 8980237]
29. Xu X, Olivas ND, Ikrar T, Peng T, Holmes TC, Nie Q, and Shi Y. (2016). Primary visual cortex shows laminar-specific and balanced circuit organization of excitatory and inhibitory synaptic connectivity. J. Physiol 594, 1891–1910. [PubMed: 26844927]
30. Takahashi T, Goto T, Miyama S, Nowakowski RS, and Caviness VS (1999). Sequence of neuron origin and neocortical laminar fate: Relation to cell cycle of origin in the developing murine cerebral wall. J. Neurosci 19, 10357–10371. [PubMed: 10575033]
31. Langevin LM, Mattar P, Scardigli R, Roussigné M, Logan C, Blader P, and Schuurmans C. (2007). Validating in utero electroporation for the rapid analysis of gene regulatory elements in the murine telencephalon. Dev. Dyn 236, 1273–1286. [PubMed: 17377980]
32. Matsuda T, and Cepko CL (2007). Controlled expression of transgenes introduced by in vivo electroporation. Proc. Natl. Acad. Sci. U. S. A 104, 1027–1032. [PubMed: 17209010]
33. dal Maschio M, Ghezzi D, Bony G, Alabastri A, Deidda G, Brondi M, Sato SS, Zaccaria RP, Di Fabrizio E, Ratto GM, et al. (2012). High-performance and site-directed in utero electroporation by a triple-electrode probe. Nat. Commun 3, 960. [PubMed: 22805567]
34. Madisen L, Zwingman TA, Sunkin SM, Oh SW, Zariwala HA, Gu H, Ng LL, Palmiter RD, Hawrylycz MJ, Jones AR, et al. (2010). A robust and high-throughput Cre reporting and characterization system for the whole mouse brain. Nat. Neurosci 13, 133–140. [PubMed: 20023653]
35. Gong S, Zheng C, Doughty ML, Losos K, Didkovsky N, Schambra UB, Nowak NJ, Joyner A, Leblanc G, Hatten ME, et al. (2003). A gene expression atlas of the central nervous system based on bacterial artificial chromosomes. Nature 425, 917–925. [PubMed: 14586460]
36. Gong S, Doughty M, Harbaugh CR, Cummins A, Hatten ME, Heintz N, and Gerfen CR (2007). Targeting Cre recombinase to specific neuron populations with bacterial artificial chromosome constructs. J. Neurosci 27, 9817–9823. [PubMed: 17855595]
37. Adesnik H. (2018). Layer-specific excitation/inhibition balances during neuronal synchronization in the visual cortex. J. Physiol 596, 1639–1657. [PubMed: 29313982]
38. Olsen SR, Bortone DS, Adesnik H, and Scanziani M. (2012). Gain control by layer six in cortical circuits of vision. Nature 483, 47–54. [PubMed: 22367547]
39. Harris JA, Hirokawa KE, Sorensen SA, Gu H, Mills M, Ng LL, Bohn P, Mortrud M, Ouellette B, Kidney J, et al. (2014). Anatomical characterization of Cre driver mice for neural circuit mapping and manipulation. Front. Neural Circuits 8, 1–16. [PubMed: 24478635]
40. Sommeijer JP, Ahmadlou M, Saiepour MH, Seignette K, Min R, Heimel JA, and Levelt CN (2017). Thalamic inhibition regulates critical-period plasticity in visual cortex and thalamus. Nat. Neurosci 20, 1716–1721.
41. Jaepel J, Hübener M, Bonhoeffer T, and Rose T. (2017). Lateral geniculate neurons projecting to primary visual cortex show ocular dominance plasticity in adult mice. Nat. Neurosci 20, 1708–1714. [PubMed: 29184207]
42. Dhillon H, Zigman JM, Ye C, Lee CE, McGovern RA, Tang V, Kenny CD, Christiansen LM, White RD, Edelstein EA, et al. (2006). Leptin Directly Activates SF1 Neurons in the VMH, and This Action by Leptin Is Required for Normal Body-Weight Homeostasis. Neuron 49, 191–203. [PubMed: 16423694]
43. Zecharia AY, Yu X, Götz T, Ye Z, Carr DR, Wulff P, Bettler B, Vyssotski AL, Brickley SG, Franks NP, et al. (2012). GABAergic inhibition of histaminergic neurons regulates active waking but not the sleep-wake switch or propofol-induced loss of consciousness. J. Neurosci 32, 13062–13075. [PubMed: 22993424]

44. Chattopadhyaya B, Di Cristo G, Higashiyama H, Knott GW, Kuhlman SJ, Welker E, and Huang ZJ (2004). Experience and activity-dependent maturation of perisomatic GABAergic innervation in primary visual cortex during a postnatal critical period. J. Neurosci 24, 9598–9611. [PubMed: 15509747]
45. Coleman JE, Nahmani M, Gavornik JP, Haslinger R, Heynen AJ, Erisir A, and Bear MF (2010). Rapid structural remodeling of thalamocortical synapses parallels experience-dependent functional plasticity in mouse primary visual cortex. J. Neurosci 30, 9670–9682. [PubMed: 20660250]
46. Rodríguez G, Chakraborty D, Schrode KM, Saha R, Uribe I, Lauer AM, and Lee HK (2018). Cross-Modal Reinstatement of Thalamocortical Plasticity Accelerates Ocular Dominance Plasticity in Adult Mice. Cell Rep. 24, 3433–3440. [PubMed: 30257205]
47. Miska NJ, Richter LMA, Cary BA, Gjorgjieva J, and Turrigiano GG (2018). Sensory experience inversely regulates feedforward and feedback excitation-inhibition ratio in rodent visual cortex. Elife 7, 1–27.
48. Gil Z, Connors BW, and Amitai Y. (1999). Efficacy of Thalamocortical and Intracortical Synaptic Connections. Neuron 23, 385–397. [PubMed: 10399943]
49. Douglas RJ, and Martin KAC (2004). Neuronal Circuits of the Neocortex. Annu. Rev. Neurosci 27, 419–451. [PubMed: 15217339]
50. Prusky GT, and Douglas RM (2003). Developmental plasticity of mouse visual acuity. Eur. J. Neurosci 17, 167–173. [PubMed: 12534981]
51. Sale A, Maya Vetencourt JF, Medini P, Cenni MC, Baroncelli L, De Pasquale R, and Maffei L. (2007). Environmental enrichment in adulthood promotes amblyopia recovery through a reduction of intracortical inhibition. Nat. Neurosci 10, 679–681. [PubMed: 17468749]
52. Vetencourt JFM, Sale A, Viegi A, Baroncelli L, De Pasquale R, O'Leary OF, Castrén E, and Maffei L. (2008). The antidepressant fluoxetine restores plasticity in the adult visual cortex. Science 320, 385–388. [PubMed: 18420937]
53. Harauzov A, Spolidoro M, DiCristo G, De Pasquale R, Cancedda L, Pizzorusso T, Viegi A, Berardi N, and Maffei L. (2010). Reducing intracortical inhibition in the adult visual cortex promotes ocular dominance plasticity. J. Neurosci 30, 361–371. [PubMed: 20053917]
54. Ribic A, Crair MC, and Biederer T. (2019). Synapse-Selective Control of Cortical Maturation and Plasticity by Parvalbumin-Autonomous Action of SynCAM 1. Cell Rep. 26, 381–393. [PubMed: 30625321]
55. Coleman JE, Law K, and Bear MF (2009). Anatomical origins of ocular dominance in mouse primary visual cortex. Neuroscience 161, 561–571. [PubMed: 19327388]
56. Akbik FV, Bhagat SM, Patel PR, Cafferty WBJ, and Strittmatter SM (2013). Anatomical plasticity of adult brain is Titrated by Nogo receptor 1. Neuron 77, 859–866. [PubMed: 23473316]
57. Park JI, Frantz MG, Kast RJ, Chapman KS, Dorton HM, Stephany C-É, Arnett MT, Herman DH, and McGee AW (2014). Nogo receptor 1 limits tactile task performance independent of basal anatomical plasticity. PLoS One 9.
58. McGee AW, and Strittmatter SM (2003). The Nogo-66 receptor: Focusing myelin inhibition of axon regeneration. Trends Neurosci. 26, 193–198. [PubMed: 12689770]
59. Freeman RD, and Olson C. (1982). Brief periods of monocular deprivation in kittens: Effects of delay prior to physiological study. J. Neurophysiol 47, 139–150. [PubMed: 7062093]
60. Lan R, Liu Q, Fan P, Lin S, Fernando SR, McCallion D, Pertwee R, and Makriyannis A. (1999). Structure-activity relationships of pyrazole derivatives as cannabinoid receptor antagonists. J. Med. Chem 42, 769–776. [PubMed: 10052983]
61. Crozier RA, Wang Y, Liu CH, and Bear MF (2007). Deprivation-induced synaptic depression by distinct mechanisms in different layers of mouse visual cortex. Proc. Natl. Acad. Sci. U. S. A 104, 1383–1388. [PubMed: 17227847]
62. Howarth M, Walmsley L, and Brown TM (2014). Binocular integration in the mouse lateral geniculate nuclei. Curr. Biol 24, 1241–1247. [PubMed: 24856206]
63. Huh CYL, Abdelaal K, Salinas KJ, Gu D, Zeitoun J, Figueroa Velez DX, Peach JP, Fowlkes CC, and Gandhi SP (2020). Long-term Monocular Deprivation during Juvenile Critical Period Disrupts Binocular Integration in Mouse Visual Thalamus. J. Neurosci 40, 585–604. [PubMed: 31767678]

64. Restani L, Cerri C, Pietrasanta M, Gianfranceschi L, Maffei L, and Caleo M. (2009). Functional Masking of Deprived Eye Responses by Callosal Input during Ocular Dominance Plasticity. Neuron 64, 707–718. [PubMed: 20005826]

65. Huberman AD, and Niell CM (2011). What can mice tell us about how vision works? Trends Neurosci. 34, 464–473. [PubMed: 21840069]

66. Priebe NJ, and McGee AW (2014). Mouse vision as a gateway for understanding how experience shapes neural circuits. Front. Neural Circuits 8.

67. Kim JE, Liu BP, Park JH, and Strittmatter SM (2004). Nogo-66 receptor prevents raphespinal and rubrospinal axon regeneration and limits functional recovery from spinal cord injury. Neuron 44, 439–451. [PubMed: 15504325]

68. Saito T. (2006). In vivo electroporation in the embryonic mouse central nervous system. Nat. Protoc 1, 1552–1558. [PubMed: 17406448]

69. Xu X, and Callaway EM (2009). Laminar Specificity of Functional Input to Distinct Types of Inhibitory Cortical Neurons. J. Neurosci 29, 70–85. [PubMed: 19129386]

70. Suter B. (2010). Ephus: multipurpose data acquisition software for neuroscience experiments. Front. Neural Circuits 4, 1–12. [PubMed: 20162034]

71. Weiler N, Wood L, Yu J, Solla SA, and Shepherd GMG (2008). Top-down laminar organization of the excitatory network in motor cortex. Nat. Neurosci 11, 360–366. [PubMed: 18246064]

72. Shepherd GMG, Pologruto TA, and Svoboda K. (2003). Circuit Analysis of Experience-Dependent Plasticity in the Developing Rat Barrel Cortex. Neuron 38, 277–289. [PubMed: 12718861]

Highlights:

- Deleting *ngr1* in L4 but not L2/3, L5, or L6, sustains OD plasticity in adult mice
- Intracortical but not thalamocortical disinhibition accompanies OD plasticity
- Blocking plasticity in L2/3 with AM-251 does not affect plasticity in L4 or L5

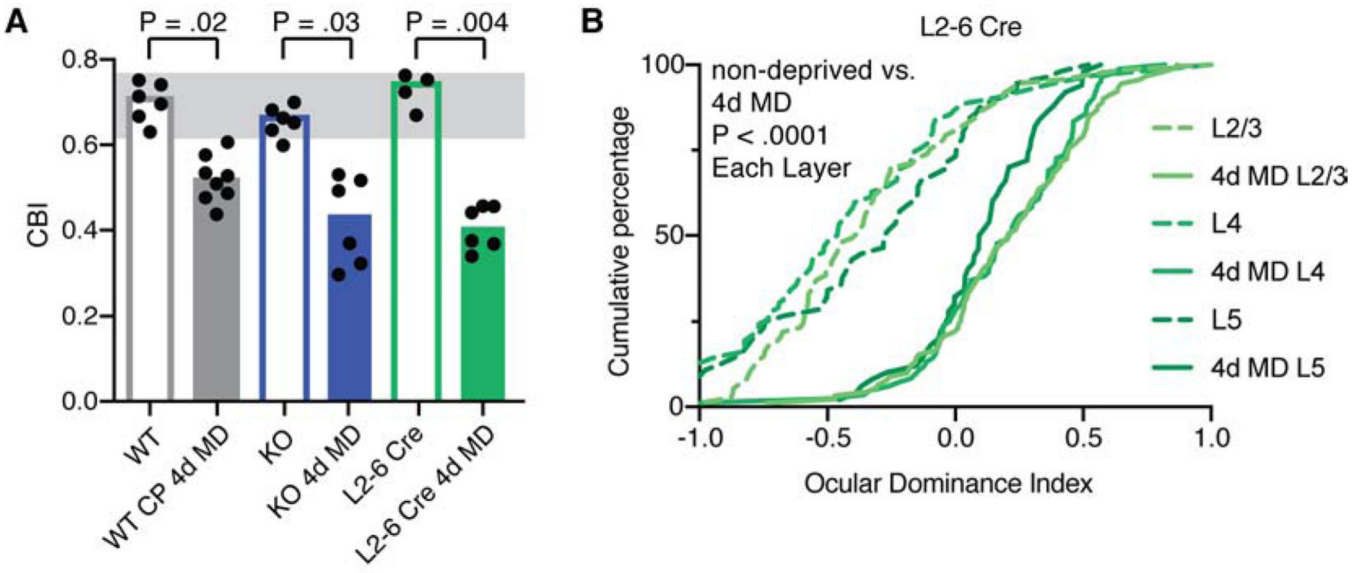

Figure 1. Selective loss of *ngr1* in forebrain is sufficient to retain OD plasticity in adult mice

(A) Contralateral Bias Index (CBI) scores for non-deprived adult WT mice (WT, n=6), juvenile WT mice following 4 days of monocular deprivation (4d MD) (WT CP 4d MD, n=8), adult non-deprived *ngr1 −/−* mice (KO, n=6), adult *ngr1 −/−* mice following 4 d MD (KO 4d MD, n=6), adult non-deprived *ngr1 flx/flx; L2–6-Cr*e mice (L2–6 Cre, n=4), and adult *ngr1 flx/flx; L2–6-Cr*e mice following 4d MD (L2–6 Cre 4d MD, n=6). Individual mice are represented as circles. The bar represents the mean of each group. The range of typical CBI values for non-deprived adult WT mice are demarcated by the grey rectangle. KW test comparing non-deprived and 4d MD for each genotype. **(B)** Cumulative distributions of units for non-deprived adult *ngr1 flx/flx; L2–6-Cr*e mice and following 4d MD for units in L2/3 (73, 91), L4 (62, 84), L5 (56, 50). MD yields a significant shift in the distribution of recorded units for each layer (P<.0001, KW test comparing non-deprived and 4d MD for each layer). See also Figure S1.

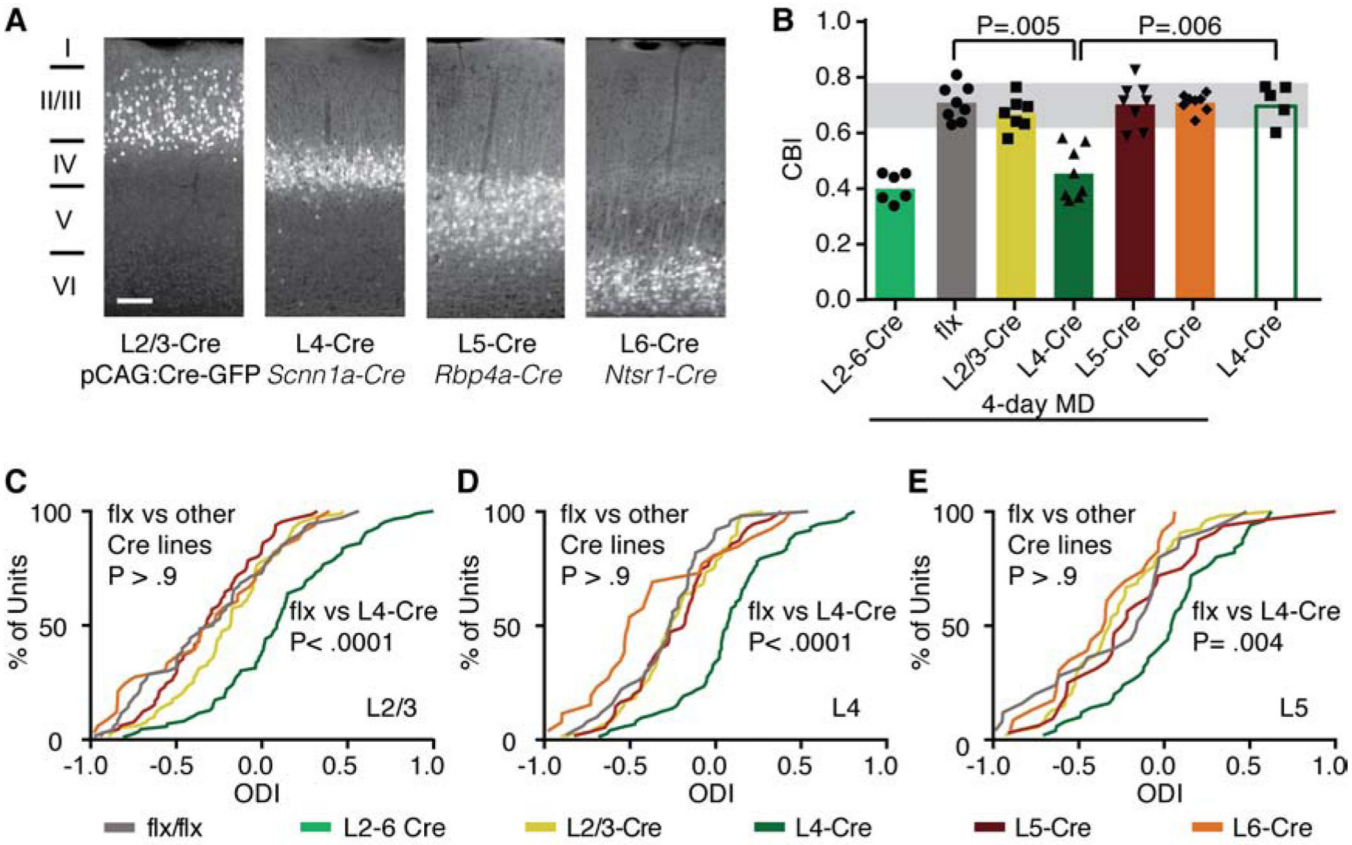

Figure 2. L4 gates OD plasticity in visual cortex through *ngr1*

(A) Layer selective activity of Cre recombinase revealed with immunofluorescent staining with antibodies directed against GFP. Coronal sections from adult *ngr1 flx/flx* mice (flx) receiving *in utero* electroporation of pCAG: CRE-GFP at E15.5 (L2/3-Cre), as well as in combination with several Cre driver lines: *Scnn1a-Tg3-Cre* (*L4-Cre*), *Rpb4a-Cre* (*L5-Cre*), and *Ntsr1-Cre* (*L6-Cre*). Scale bar, 100 microns. Relative positions of each cortical layer are indicated on the left. **(B)** CBI scores for adult, *ngr1 flx/flx; L2/3-Cr*e mice (L2/3-Cre, n=7), *ngr1 flx/flx; L4-Cr*e mice (L4-Cre, n=8), *ngr1 flx/flx; L5-Cr*e mice (L5-Cre, n=8), and *ngr1 flx/flx; L6-Cr*e mice (L6-Cre, n=8) following 4 days of MD, as well as non-deprived adult L4-Cre mice (n= 5). The *ngr1 flx/flx; L2–6-Cr*e mice (L2–6 Cre, n=6) from Figure 1 are shown for reference. CBI scores for *L4-Cre* mice following 4d MD are significantly lower than both *flx* alone mice after MD (P=.005) as well as non-deprived *L4-Cre* mice (P=.006), whereas flx alone is not significantly different from L2/3-Cre, L5-Cre or L6-Cre (KW test). The bar represents the mean of each group. The range of typical CBI values for non-deprived adult WT mice from Figure 1 are demarcated by the grey rectangle. **(C-E)** Cumulative distributions of units for the genotypes and deprivation conditions in (B) classified according to layer (n=units). **(C)** L2/3: flx (96), L2/3-Cre (80), L4-Cre (86), L5-Cre (88), and L6-Cre (85) **(D)** L4: flx (61), L2/3-Cre (60), L4-Cre (73), L5-Cre (70), and L6-Cre 66) **(E)** L5: flx (29), L2/3-Cre (54), L4-Cre (50), L5-Cre (40), and L6-Cre (45). L4-Cre is significantly different from flx for each layer (P=.004 or lower, KW test). See also Figure S2.

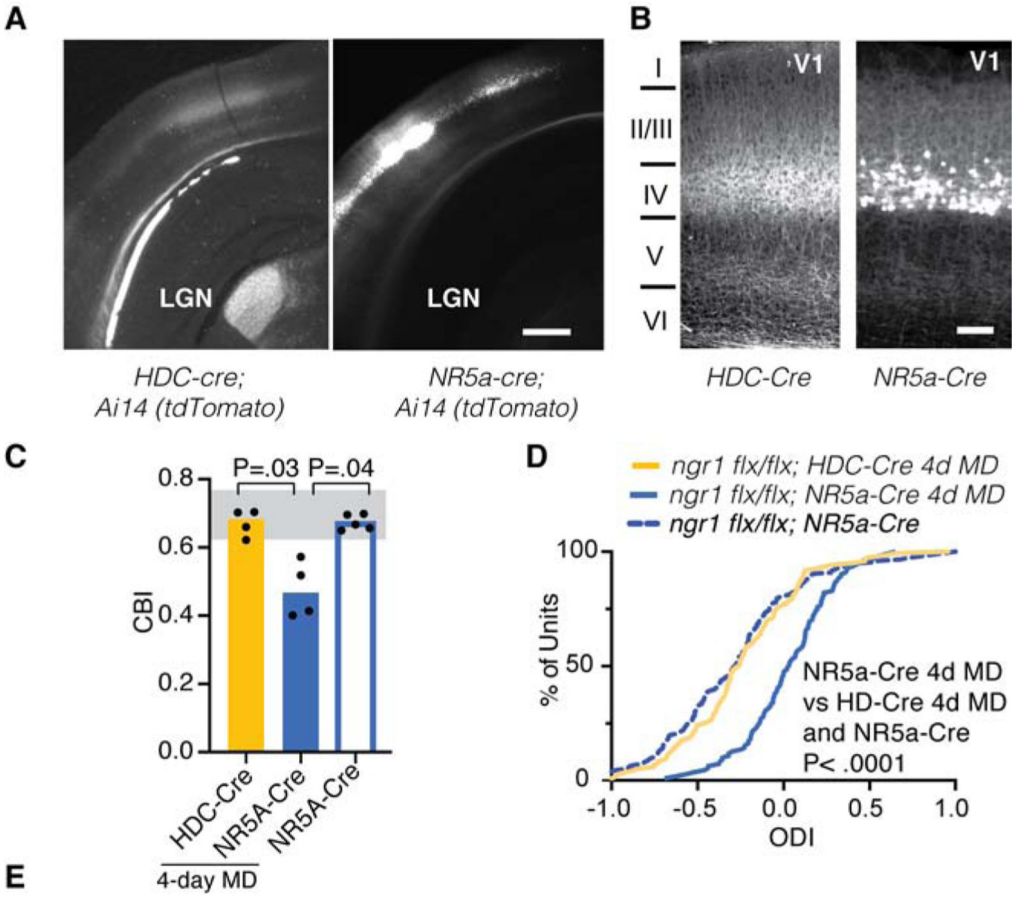

E

Cre Driver	Expression	% Excitatory Cortical Neurons	OD Plasticity L2/3	L4	L5
CamK2a-Cre	L2-6	~ 100% (?)	+	+	+
pCAG:Cre-GFP	L2/3	~ 30%	-	-	-
Scnn1a-Tg3-Cre	L4 + LGN	~ 60%	+	+	+
NR5a-Cre	L4	~ 30%	+	+	+
Rpb4a-Cre	L5	~ 40%	-	-	-
Ntsr1-Cre	L6	~ 65%	-	-	-
HDC-Cre	LGN	0%	-	-	-

Figure 3. Deletion of *ngr1* in L4 with a distinct Cre driver also sustains OD plasticity in adult mice

(A) Coronal sections of adult mouse brain from *HDC-Cre* (left) and *NR5a-Cre* (right) in combination with the Cre reporter *Ai14 (tdTomato).* Cell soma labeled with red fluorescence are evident in the lateral geniculate nucleus (LGN) in *HDC-Cre* mice and in L4 of *Nr5a-Cre* mice. Scale bar = 0.5mm **(B)** Higher magnification images of coronal sections of visual cortex from these same genotypes. Scale bar, 100 microns. Relative positions of each cortical layer are indicated on the left. *HDC-Cre* section is oversaturated to highlight

thalamocortical axons. **(C)** CBI scores for *ngr1 flx/flx; HDC-Cre* (n=4 mice) and *ngr1 flx/flx; Nr5a-Cre* (n=4 mice) following 4 days of MD and non-deprived *ngr1 flx/flx; Nr5a-Cre* (n=5 mice). The range of typical CBI values for non-deprived adult WT mice from Figure 1 are demarcated by the grey rectangle. CBI scores for *ngr1 flx/flx; Nr5a-Cre* mice following MD are significantly lower than those of *ngr1 flx/flx; HDC-Cre* mice after MD and non-deprived *ngr1 flx/flx; Nr5a-Cre* mice (P = .022 and .0391, respectively, KW test). **(D)** Cumulative distributions of units for these same mice (n=units): *HDC-Cre* 4d MD(120), *Nr5a-Cre* 4d MD (111), *Nr5a-Cre* non-deprived (166). Nr5a-Cre 4d MD is significantly different from HDC-Cre 4d MD and *Nr5a-Cre* non-deprived (both P<.0001, KW test). (E) The layer of Cre expression, the estimated percentage of excitatory cortical neurons expressing Cre, and whether Cre expression permitted (+) or did not permit (−) OD plasticity in adult mice in each layer for mice with deletion of *ngr1* restricted by IUEP or a Cre driver line. OD plasticity by layer for *NR5a-Cre* is data not shown. See also Figure S3.

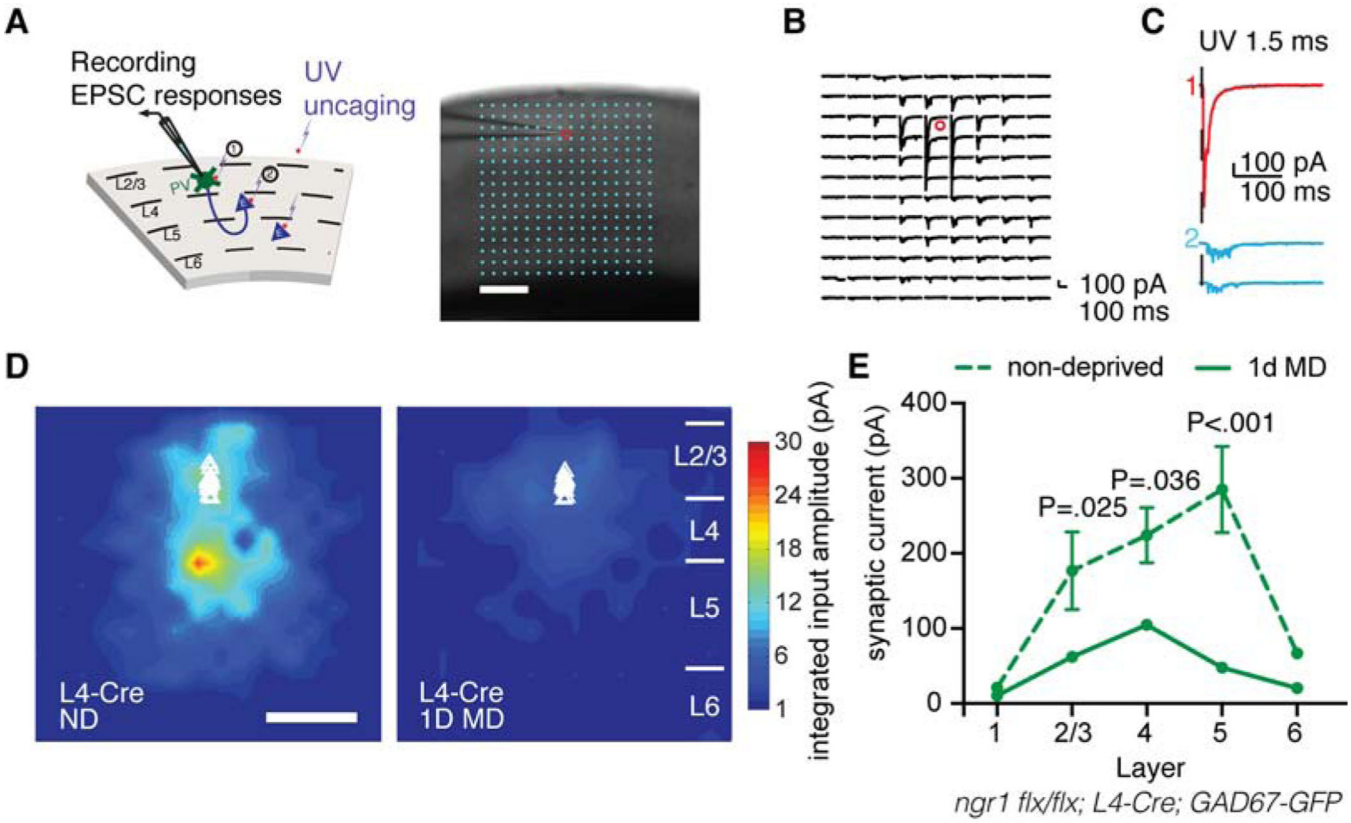

Figure 4. Deletion of *ngr1* in L4 permits intracortical disinhibition with 1-day MD in adult mice

(A) Schematic of the recording configuration. PV interneurons expressing GFP directed are patched in the whole-cell configuration. A UV laser directs the focal release of glutamate over the soma of excitatory neurons distributed throughout the tissue section. Glutamate uncaging drives the firing of APs by neurons under the region of brief UV illumination. **(B)** An example of the 16×16 grid (aqua dots) and the position of a recorded PV interneuron on L2/3 (red circle). **(C)** An example of the current induced by direct somatic stimulation (1, red trace, upper) of the recorded PV interneuron, and excitatory synaptic currents (2, blue trace, lower). **(D)** LSPS mapping of excitatory synaptic inputs onto PV interneurons in L2/3 of adult (P55-P65) *ngr1 flx/flx; L4-Cre; GAD67-GFP* mice (non-deprived (ND) n=10 cells, 1-day (1d) MD n=16 cells). Relative positions of each cortical layer are indicated on the right. These mice display a loss of excitatory drive with 1d MD similar to during the critical period. **(E)** Average excitatory synaptic input to L2/L3 PV interneurons by layer for non-deprived mice and after 1d MD. Synaptic current per layer is plotted as mean ± SEM. Synaptic current is significantly lower from L2/3 (P=.025), L4 (P=.036), and L5 (P <.001) following MD (Two-way RM ANOVA, Sidak's multiple comparison test). See also Figure S4.

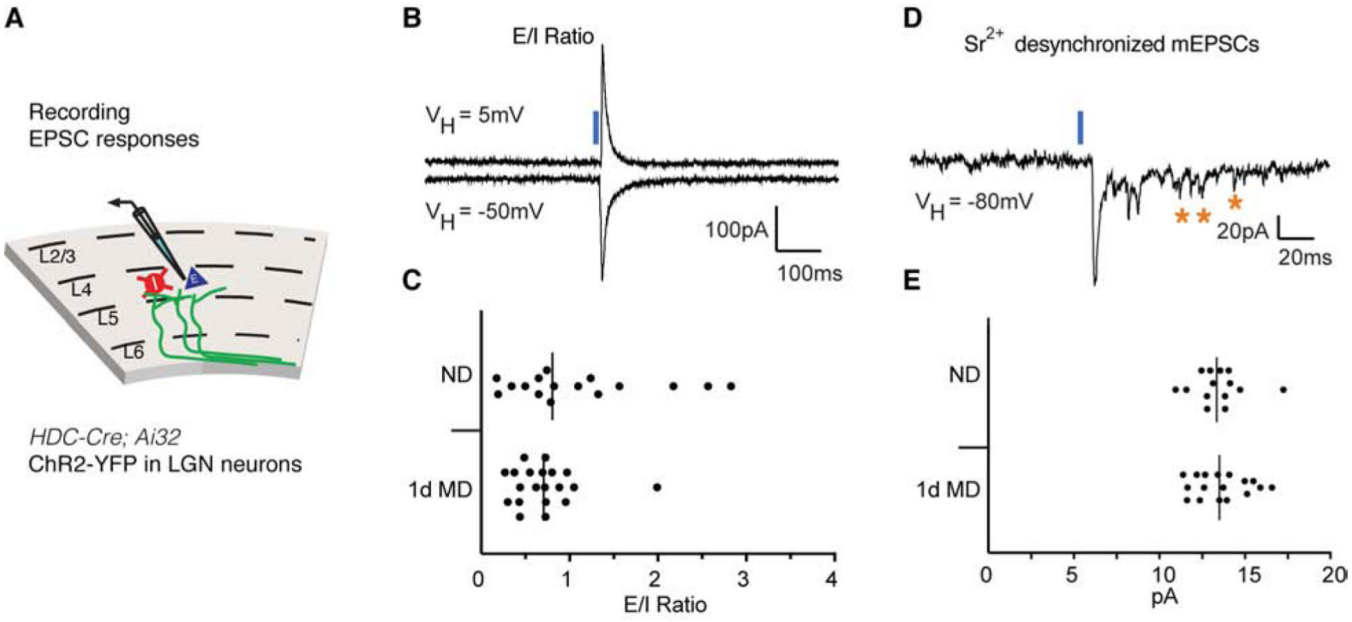

Figure 5. Thalamocortical E/I ratio and mEPSC amplitude are unaltered by 1-day MD

(A) Schematic of the recording configuration. Pyramidal excitatory neurons in L4 of visual cortex of juvenile (P26–30) wild-type *HDC-Cre; Ai32 (ChR2-YFP)* mice are patched in the whole-cell configuration. Thalamic axons projecting into V1 express ChR2-YFP. **(B)** Example traces of direct responses recorded at a holding potential of −50mV; disynaptic inhibitory currents are recording at a holding potential of 5mV. Synaptic release is evoked with a 5ms pulse of blue light (blue line). **(C)** Neurons from non-deprived (ND) mice (n = 16) and mice after 1 day (1d) of MD (n=20) display similar E/I ratios (P=.147, MW test). **(D)** Example traces optogenetic-evoked putative thalamocortical mEPSCs desychronized by the presence of Sr^{2+}. The light pulse is indicated by the blue line. Gold asterisks identify mEPSCs. **(E)** Neurons from non-deprived (ND) mice (n = 14) and mice after 1d of MD (n=17) display similar mEPSC amplitudes (P=.89, MW test). See also Figure S5.

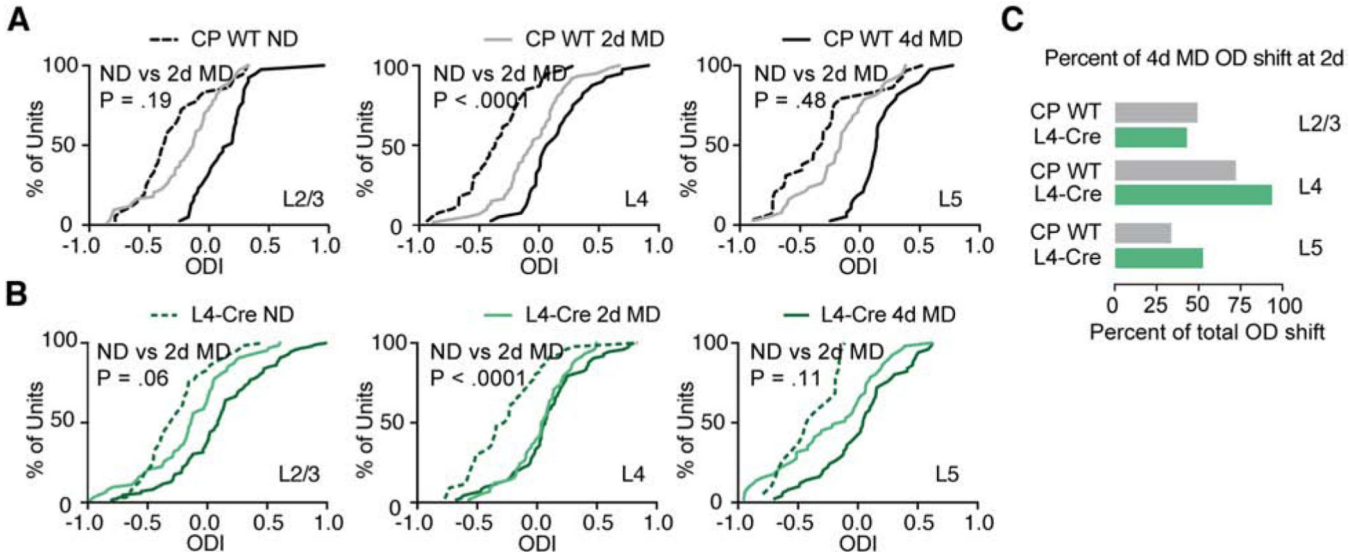

Figure 6. OD plasticity is first detectable in L4 in juvenile WT and adult *ngr1 flx/flx; L4-Cre* mice

(A) Cumulative distributions of ODI values for units in L2/3 (left), L4 (middle), and L5 (right), for non-deprived critical period (CP) WT mice (ND, dashed line) and following 2 days of MD (2d MD, light grey line) and 4 days of MD (4d MD, dark grey). Units per layer in parentheses, L2/3: ND (36), 2d (73), 4d (39); L4: ND (39), 2d (60), 4d (40); L5: ND (29), 2d (38), 4d (38). Statistical comparison is a KW test comparing all combinations of ND, 2d MD, and 4d MD for each layer. **(B)** Cumulative distributions of ODI values for units in L2/3 (left), L4 (middle), and L5 (right), for non-deprived adult *ngr1 flx/flx; L4-Cre* mice (ND, dashed line) and following 2d MD (2d MD, light green) and 4d MD (4d MD, dark green). Units per layer in parentheses, L2/3: ND (57), 2d (63), 4d (86); L4: ND (44), 2d (58), 4d (73); L5: ND (19), 2d (51), 4d (50) Statistical comparison is a KW test comparing all combinations of ND, 2d MD, and 4d MD for each layer. **(C)** The percentage of the total OD shift per layer between non-deprived mice and after 4d of MD achieved by 2d of MD for both CP WT mice and adult *ngr1 flx/flx; L4-Cre* mice. See also Figure S6.

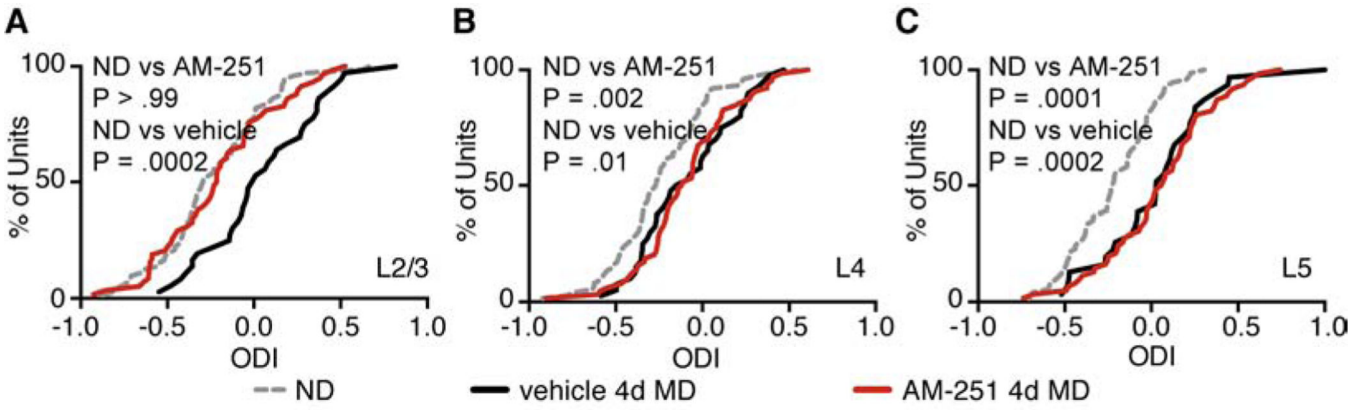

Figure 7. OD plasticity in L5 does not require OD plasticity in L2/3

Cumulative distributions for units per layer for juvenile WT mice either non-deprived (ND) or after 4 days (4d) of MD during treatment with AM-251 or vehicle (n=units). **(A)** AM-251 blocks OD plasticity in L2/3 as AM-251 treated (58) is not significantly different from ND (73) (P>.99) while vehicle is significantly shifted towards the open eye (36) (P=.0002, KW test). **(B)** AM-251 does not affect OD plasticity in L4 as both AM-251 treated (75) and vehicle treated (40) are significantly different than ND (64) (P=.002, P=.01, respectively, KW test). **(C)** AM-251 does not affect OD plasticity in L5 as both AM-251 treated (74) and vehicle treated (31) are significantly different than ND (62) (P=.0001, P=.0021, respectively, KW test). See also Figure S7.

KEY RESOURCES TABLE

REAGENT or RESOURCE	SOURCE	IDENTIFIER
Antibodies		
Rabbit polyclonal anti-GFP	Novus	Cat#NB600-308; RRID: AB_10003058
Rabbit polyclonal anti-PV	R&D Systems	Cat#AF-5058; RRID:AB_2173907
Chemicals		
AM-251	Tocris Bioscience	Cat#1117
MNI-caged-L-glutamate	Tocris Bioscience	Cat#1490
SR 95531 HBr	Tocris Bioscience	Cat#1262
(RS)-CPP	Tocris Bioscience	Cat#0173
TEA-Cl	Tocris Bioscience	Cat#3068
2-Chloroadenosine	Tocris Bioscience	Cat#3136
QX-314	Sigma-Aldrich	Cat#552233
Experimental Models: Organisms/Strains		
Mouse: C57Bl6J - rtn4r KO	[67]	N/A
Mouse: C57Bl6J - rtn4r flx	[25]	N/A
Mouse: C57Bl6J	The Jackson Laboratory	JAX: 00664
Mouse: B6.Cg-Tg(Camk2a-cre)T29-1Stl/J	The Jackson Laboratory	RRID:IMSR_JAX: 005359
Mouse: B6.Cg-*Gt(ROSA)26Sor*$^{tm14(CAG-tdTomato)Hze}$/J	The Jackson Laboratory	RRID:IMSR_JAX: 007914
Mouse: B6;C3-Tg(Scnn1a-cre)3Aibs/J	The Jackson Laboratory	RRID:IMSR_JAX:009613
Mouse: Tg(Rbp4-cre)KL100Gsat/Mmucd	MMRRC	RRID:MMRRC_031125-UCD
Mouse: B6.FVB(Cg)-Tg(Ntsr1-cre)GN220Gsat/Mmucd	MMRRC	RRID:MMRRC_030648-UCD
Mouse: Tg(Nr5a1-cre)7Lowl/J	The Jackson Laboratory	RRID:IMSR_JAX:012462
Mouse: HDC(tm1.1(icre))Wwis/J	The Jackson Laboratory	RRID:IMSR_JAX:021198
B6.Cg-Gt(ROSA)26Sortm32(CAG-COP4*H134R/EYFP)Hze/J	The Jackson Laboratory	RRID:IMSR_JAX:024109
Oligonucleotides		
Ngr1 WT F: cag tac ctg cga ctc aat gac	[67]	N/A
NgR1 WT R: ctt ccg gga aca acc tgg cct cc	[67]	N/A
Neo F: ta ttc ggc tat gac tgg gca	[67]	N/A
Neo R: gaa ctc gtc aag aag gcg ata	[67]	N/A
CRE F: ccg gtc gat gca acg agt gat gag gtt cgc	[26]	N/A
CRE R: ctc gac cag ttt agt tac ccc cag gct aag	[26]	N/A

REAGENT or RESOURCE	SOURCE	IDENTIFIER
NgR1 flx R: gcg gat ctt gaa gtt cac ctt	[26]	N/A
NgR1 flx/WT F: gag ctg aca tcc atg agc tca gcc	[26]	N/A
NgR1 WT R: ggg aga cag acc cat tcc tgg tcc ctc aca acc	[26]	N/A
NgR1 delta F: tgg tga cca att ggg cta gcc ctg tgg	[26]	N/A
Recombinant DNA		
pCAG-Cre:GFP	Addgene	RRID:Addgene_13776
Software and Algorithms		
Spike2 Software	CED	RRID:SCR_000903
MATLAB	Mathworks	RRID:SCR_001622
MATLAB visual stimulus scripts	[21]	N/A
MATLAB LSPS scripts	[69]	N/A
pClamp	Molecular Devices	RRID:SCR_011323
Mini Analysis Program	Synaptosoft	RRID:SCR_002184
Prism 8	GraphPad	RRID:SCR_002798
Primary data		
https://data.mendeley.com/datasets/2xz34tkxmf/draft?a=1583d81c-4d4d-418d-8337-2ef331ba127b		